Università degli Studi di Napoli Federico II


Doctorate course in
Materials and Structures Engineering
*Doctoral thesis*

# Engineered microfluidic platforms for microenvironment control and cell culture

Coordinator:
Prof. Giuseppe Mensitieri

Candidate
Gabriele Pitingolo

Supervisors:
Prof. Paolo Antonio Netti
Eng. Raffaele Vecchione Ph.D.

# Table of Contents

# Abstract

The aim of this thesis is to overcome present limitations in mimicking the in vivo cellular microenvironments with novel *in vitro* cell culture systems. Since microtechnologies and microfluidics, in particular, provide the tools to reproduce *in vivo*-like cellular microenvironments *in vitro*, current relevant research is presented and areas where more research is needed in characterizing the *in vitro* microenvironment are outlined. 2D and 3D dynamic cell-culture models have recently garnered great attention because they often promote levels of cell differentiation and tissue organization not possible in conventional 2D static culture systems. In this work we developed new microfabrication approaches to reproduce cell-culture microenvironments that both support tissue differentiation and recapitulate the tissue–tissue interfaces, spatiotemporal chemical gradients, and mechanical microenvironments of living systems. These 'tissues-on-chips' permit the study of human physiology in physiological contest, enable development of novel *in vitro* disease models, and

could potentially serve as replacement for animals used in drug development and toxin testing. To this aim, a blood brain barrier (BBB) microfluidic device was designed based on a transparent polyester porous membrane sandwiched between a top and a bottom overlying channel made of PMMA. According to our results, the PMMA is the most suitable biocompatible material for the porous membrane integration between two layers, compared to other materials, such as PDMS, commonly used to fabricate similar devices. We faced its permeability issue by engineering the proposed device with a collecting chamber, in the top part, to ensure the oxygen provision. In order to verify the efficacy of this microfluidic system, we tested the passage of BSA and nanoparticles compared to blank porous filter. Afterwards, in order to better mimic the blood-brain barrier and its circular shape we developed an innovative method to fabricate miniaturized circular microchannels from square geometry. A wide range of perfusable microvessel models have been developed, exploiting advances in microfabrication, microfluidics, biomaterials, stem cell technology, and tissue engineering. These models vary in complexity and physiological relevance,

but provide a diverse tool kit for the study of vascular phenomena and methods to vascularize artificial organs. Here we developed a fast, cheap and reproducible method to fabricate circular microchannels by coupling spin coating with micromilled square microchannels. In order to validate our approach, an endothelial cell layer was formed by culturing brain endothelial bEnd.3 cells inside the proposed circular microchannels. In addition, considering that the diameter of blood vessels, in humans, spans more than four orders of magnitude, from about 8 µm in capillaries to more than 1 cm in large elastic arteries, we developed a low cost approach, using gelatin dehydration as intermediate, to fabricate microchannels of 5-8 microns in width, in order to mimic smaller capillaries. We are currently exploring the possibility to apply our approaches to fabricate a 3D microvessel model, totally in gelatin, to better mimic the extracellular matrix and the endothelium. In parallel, associated with the development of the above described devices, we proposed practical tips to the miniaturization community, developing innovative techniques that offer a solution to commonly encountered problems in the microfabrication field, or improvements (e.g.

a simplification) on existing techniques. Thanks to their cost and technical advantages these microfluidic platforms may have extensive applications for neurobiology, cancer biology and for studying the cell-biomaterial interaction.

# List of figures

# Ethical design

Ethical considerations can be specified as one of the most important parts of this manuscript. Ethics was applied on all stages of this research, such as planning, conducting and evaluating. The first thing done before designing a study is to consider the potential cost and benefits of the research. To this aim, the use of human/mouse derived cells in *in vitro* models, or especially in microfluidics system, can make them more representative of the human response to NPs as opposed to animal models. As a result of the rapid expansion in the use of nanoparticles (NPs) in recent years, it is imperative that we advance our understanding of NP interactions with biological systems in order to establish safety standards and improve the design of nanomaterials. Such mechanisms can of course be investigated in *in vivo* systems, however the demand and need for *in vitro* experimental models is increasing. The new international legislation designed to limit the use of animal models in toxicological studies in industrial settings, so researchers are

being forced to design and validate novel *in vitro* methods to perform these experiments. Many innovative methods have been, recently, used to develop new models and improve existing ones. In comparison to *in vivo* systems, they are generally faster to run, more cost effective and often relatively simple thus allowing for well controlled experiments with easily interpreted results. These features make them ideal for developing large scale screening researches, which is of interesting value for the field of nanotechnology considering the huge numbers of new NPs varying in shape, composition, dimension and formulation etc. To summarize, the proposed *in vitro* models provide a new beneficial tool, as alternative methods, for the study of NP interactions with biological systems.

# Introduction

2D and 3D 'tissues-on-chips' are microengineered biomimetic systems,[1] containing microfluidic channels lined by living human cells,[2] or animal cells functionally similar to the human ones, which replicate key functional units of living organs to reconstitute integrated human organ-level pathophysiology in dynamic in vitro models.[3] These microfluidic devices can be used to test efficacy of nanocarriers to cross biological barriers, to study the toxicity of encapsulated drugs in nanocarriers and to provide in vitro models of human disease.[4] Thus, they potentially represent ethical and cost effective alternatives to conventional animal models for pharmaceutical, chemical and environmental applications. In this contest microfluidics, a micro-technological field that deals with the handling of fluids and dispersions of nano and micro-objects, currently applied in biological, biomedical, and chemical analyses, has offered tremendous novelty over the last two decades. Under the framework of 'lab-on-a-chip', 'micro-total-analysis system (μTAS)' or 'bio-micro-electro-mechanical system (bio- MEMS)', various microfluidic systems

have been developed for biological investigations.[2] Microfluidic devices have many advantages over traditional system, such as low cost, low reagent consumption, fast experiment time, and high-throughput analysis, which have been utilized for cellular assays. One important class of microfluidic devices are those for cell culture and microenvironment control to interrogate cellular behaviors in specified physiological microenvironments, which are not readily achievable in conventional bulk systems. For this aspect we developed a new blood brain barrier (BBB) microfluidic model to overcome the limits of those previously developed, in terms of fabrication times and immobilization of the porous membrane.[5] To verify our issue, we first characterized the growth and the formation of a confluent brain endothelial layer. Then, the permeability of this system was tested by using fluorescent albumin (BSA) as a standard molecule and other nanoparticles as a control indicating the functionality of our model. Finally, the capability of conjugated nanoparticles to adhere to and cross the brain endothelial layer under flow conditions was investigated. Recent advances in microengineering technologies, however, have made it

possible to considerably improve rudimentary static models. This has led to the development of much more sophisticated microfabricated devices that allow one to study tissue-tissue interfaces, along with complex organ-specific chemical and mechanical microenvironments, to mimic key 3D functional units of living human organs.[6, 7] Various approaches to fabricate these devices have been reported depending on the end goal of industrial mass production or rapid prototyping at the research laboratory level, including photolithography coupled with wet etching, reactive ion etching, stamp based techniques, such as soft lithography, hot embossing and injection molding, as well as ablating technologies like conventional machining, laser ablation and finally direct 3D printing. [8] Nowadays, the available techniques to make small and circular microchannels are cost expensive and time consuming.[9, 10] Working on this direction we developed an innovative low cost method to fabricate circular and smaller microchannels to mimic *in vitro* the microvessels. To validate our system, we cultured cells inside the proposed microdevices. In the first step we used PDMS to fabricate the microvessel, subsequently we started to develop an advanced

microvessel model using as biomaterial an hydrogel that is more biocompatible and better resemble the in vivo system. The general conformation and geometry of the microdevices fabricated with different technologies were characterized using optical microscopy, scanning electron microscopy (SEM) and a surface profilometer, while AFM was used to characterize channel roughness. Cell constructs were observed and images were acquired by multiphoton confocal microscope (Leica TCS SP5 MP) equipped with different objectives.

# 1 Microfluidic Platforms for Cell Culture

## 1.1 Mechanical forces

Cells cultured in macro and micro systems face the risk of being exposed to mechanical forces from fluid motion and/or bubbles.[11] In classical *in vitro* systems, stirring is necessary to evenly distribute nutrients, but the resulting fluid motion can cause shear damage to cells. Bubbles, necessary for aeration of the culture volume, cause damage to cells principally when they burst—cells caught at the air/medium interface of the bubble can rupture when the bubble collapses. In microfluidic channels, stirring is not necessary to evenly distribute nutrients and minimize waste accumulation. A common useful method is to flow medium past cells adhered within the microchannel.[12] This causes shear on the cells, but through a correct microsystem design, the shear can be minimized. Bubbles are not necessary for aeration in microsystems if gas permeable polymers are used as the construction material for the microdevice, for example PDMS or large open chambers.[13] Assuming the polymer is adequately permeable, diffusion will

be able to effectively exchange oxygen and carbon dioxide with the medium in the microdevice. However, bubbles can form in microchannels during filling or pumping. When a bubble is formed in a microchannel within a gas-permeable polymer, it can grow as a result of the lower air pressure created from fluid inside the microchannel. Bubbles often grow until they occlude the microchannel and impede flow. Cells that come into contact with bubbles in microfluidic channels are subject to the same stresses present in macroscale systems. The third way mechanical forces might adversely affect cells in microchannels is through physical deformation within the microfluidic device, either intentional or from poor device design. For example, some experiments may require a cell to be physically restrained for treatment or analysis. The cell may become deformed by fluid forces and/or the microstructures restraining the cell (e.g., posts or sieves). The effect of fluid and physical forces on cell behavior must be taken into account when designing microenvironments.

## 1.2 Shear effects

Shear stress occurs when an object undergoes a tangential force. In microfluidics systems, the shear stress present throughout a microchannel can be represented mathematically with Newton's law of viscosity

[eqn. (1)]

$$\tau = -\mu \frac{\mathrm{d}v}{\mathrm{d}x} \tag{1}$$

where τ is the shear stress, μ is the fluid viscosity, v is the fluid velocity, and x is the position within the channel. Fig. 1 shows the profiles of velocity into two microchannels with different heights. The flows in both microchannels have the same maximum velocity, but the smaller channel has a larger change in velocity over x (i.e., the smaller channel has a larger value for dv/dx). Therefore, for a given maximum fluid velocity the shear stresses present in a smaller microchannel are greater than those in a larger microchannel.

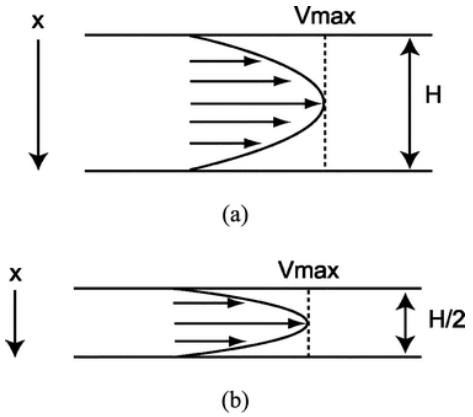


Fig. 1.Velocity profiles for different microchannels (a) A velocity profile for a channel of height H and maximum velocity $V_{max}$. (b) If the channel is half as tall, and the maximum velocity is still $V_{max}$, the rate of change in velocity over x is much greater than in (a). Walker et al., Lab on a Chip 2004

This aspect of shear stresses is important when designing microscale cell culture systems that will require fluid flow. Furthermore, for several cell lines the medium replacement is needed to meet the high nutrient requirements (e.g., mammalian). The maximum shear that can be endured by the cells will depend on the cell line types, for example endothelial cells require shear stress to develop properly and others are affected by shear stress, even though their phenotype does not change.[14] Experimental research in shear stresses on cells

has typically been used for the study of leukocyte adhesion and endothelial cell responses (i.e., mechanotransduction).[15] More research on cellular responses to shear stress within microchannels is needed, especially outside the context of blood flow studies.

**Shear on single cells**. Analytical aspects to the forces experienced by a sphere in a fluid have been known for over four decades. The pioneers of the shear stress concept on single cells, Gaver and Kute, have shown that the shear stress degree on a cell in a microchannel with pressure-driven flow is greater than that predicted by shear stress calculations in a no-cells microchannel. The Gaver and Kute model assumed a cell of radius R was attached to the bottom of a microchannel of length $L_c$ and height $H_c$ (Fig. 2). [16] Through regression analysis, they have found the method to calculate flow rate, maximum shear stress, force on the cell, and torque. They also showed that the maximum shear stress on a cell is amplified by an amount inversely proportional to the cell size-to-channel height ratio. Design considerations from Gaver and Kute for cells in microchannels with pressure-driven flows are:

(1) Assuming $R/L_c = 0.01$, the volumetric flow rate within the microchannel is not impeded until $R/H_c > 0.3$; (2) Assuming $R/H_c = 0.1$, a cell within the microchannel experiences an amplified shear stress by a factor of 3.0, force by a factor of 3.0, and torque by a factor of 1.2 with respect to values for flow in a cell-free microchannel; (3) In general, the cell radius should be a small fraction of the channel length and height.

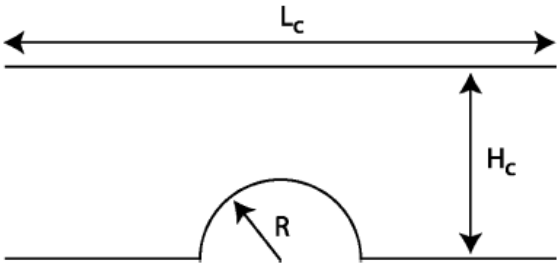


Fig. 2. Shear stress on a single cell. A cell was modeled as a semicircle of radius. Walker et al., Lab on a Chip 2004

**Shear stress on multiple cells**. When many cells are cultured in a microchannel, intercellular space plays an important role in determining the fluid forces on each cell. A recent model for determining the influence of cell space on fluid flows has been developed by Sugihara-Seki. Sugihara-Seki used a model that

assumed attached cells of radius, R, were in a channel of height 2H and were separated from their nearest neighbor by a distance of 2L (Fig. 3).[16, 17] Important design considerations from Seki's analysis are: (1) If L/2 >> H then cells do not affect the flow field around their neighbors; (2) For R/H > 0.3, cells in tubes experience greater drag from flow than cells between parallel plates; (3) If L/H > 1.5, the drag and torque on a cell are not influenced by its neighbor.

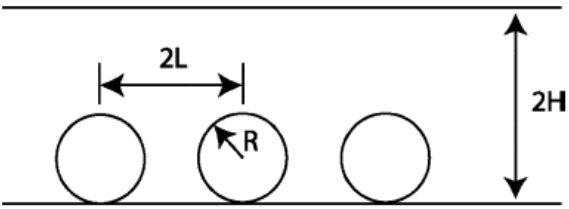


Fig. 3. Shear stress on multiple cells. Multiple cells 2L apart and of radius R were modeled as spheres along the bottom of a tube of radius H. Walker et al. Lab on a Chip 2004

**Surface area to volume ratio.** Very large surface area to volume (SAV) ratios are advantageous in cell culture systems mainly because of efficient mass transport of gases via diffusion to and from cells, for this reason is better the use of gas-permeable polimer to fabricate microchannels. Cells at the

macroscale are often cultured in culture dishes with a low (SAV) ratios. For example, a 35 mm tissue culture dish with 1 mL of medium in it has a SAV of 11 $cm^{-1}$. [18] Cells cultured in a microfluidic channel with dimension 50 x 50 µm x 3 cm (H x W x L), corresponding to a volume of 75 nL, are in an microenvironment with a SAV of 800 $cm^{-1}$. [19]

**Effective culture volume.** Generally, the aspects of macroscale bioreactor design are not directly applicable to microfluidics cell culture. Designing a microfluidic cell culture environment requires taking into consideration the physical aspects of the microscale. [20]For example, in a traditional cell culture flask cell volume/medium volume ratios are << 1, the SAV is very small, and the fluid environment is characterized by large a Pe. In contrast, microfluidic channels environments have a cell volume/medium volume ratio close to one, a very large SAV, and a small Pe. As a step towards characterizing cell culture microenvironments, it is introduced the concept of an "effective culture volume" (ECV). The ECV is an indicator of the cell's ability to control its microenvironment during culture. The ECV is a function of the magnitude of mass

transport along each axis, the effects of diffusion and convection (Pe), and the degree of protein adsorption to surfaces. For example, the ECV of a cell in a microchannel is characterized by mass transport limited to one dimension—the x axis (diffusion distances are short along the along the y- and z axes). Protein adsorption is likely to be present because of the large SAV, but can be minimized by treating the microchannel surfaces, as discussed later. A cell in a tissue culture flask sees a different environment (Fig. 6b). Convective and diffusive transport can occur equally along all three axes and protein adsorption is not likely to be a problem since the SAV is so small. Cells in microscale culture have better control over their local environments than cells in macroscale culture, thus the ECV at the microscale is smaller than at the macroscale. In vivo environments are defined by small ECVs. However, much work is still needed to empirically determine relationships between different ECVs and their effect on cell behavior.[21]

## 1.3 Material interfaces

Material interfaces have multiple influences on microfluidic culture environments. Interfaces exist between the cell and chemical-physical elements, such as solid and liquid, as well as between the culture medium and walls and gases. Due in large part to the phenomena previously discussed, evaluations at the microfluidic environment are important for the understanding of cellular interactions and responses within microenvironment conditions. Material interfaces play a significant role in microscale culture because of the large SAV ratios present.[13]

**Surface adsorption**. Surface adsorption is the phenomenon of molecules superficially adhering to a surface. In a cell culture environment, this is predominantly seen where the medium contacts the chamber walls. Due to the large SAV ratio seen in microscale culture, surface adsorption becomes an important design consideration. Proteins in culture medium have wide-ranging effects on a cell and are often internally hydrophobic. Many materials used in the fabrication of micro culture

environments are also hydrophobic, though much work has been done on surface modification for biocompatibility.[22, 23] The hydrophobic protein interior will be attracted to a nearby hydrophobic microchannel wall, causing the protein to denature at the medium/wall interface. Because denatured proteins will disengage from the chamber wall after a period of time, chamber walls can become a constant sink for medium proteins. Depletion of medium protein concentrations through protein adsorption affects subsequent culture conditions. In traditional culture, the relatively small surface area does not cause drastic alterations of medium by protein denaturation. In microscale culture conditions, the high SAV ratios can cause significant protein depletion.

**Cell adhesion.** One of the most important and relevant effects of a cell's immediate environment is its interaction with supporting substrate. The microscale relationship of cellular structure with external supporting substrate can influence many cellular characteristics, including adhesion strength, orientation, cytoskeletal structure, growth, death, and others.[24-28] Cells typically adhere to substrates via focal

adhesion complexes (FACs), which are conglomerates of proteins on the cell surface.[29, 30] The substrate and its shape help determining the proteins used for adhesion. [29] Different compositions of FAC proteins have different effects on cytoskeletal structure. Regardless, microtechnologies allow an increasingly precise determination of cell adhesion phenomena. Microscale substrate patterning allows investigation of a cell's adhesion response to different substrates. Micropatterning can be used to geometrically define where specific cells will adhere to a particular substrate and the placement and degree of cell–cell contact. Micropatterning of adhesive spots on the size scale of FACs has allowed a more specific examination of how FACs work and the conditions involved in their assembly. Teixeira et al. have explored the effect of nanoscale texture on cell adhesion. Previous studies used varied surface chemistries to achieve differing substrate dimensions. Teixeira used silicon micromachining to achieve equivalent surface chemistries across a wide range of topographical dimensions. Cellular adhesion and orientation was correlated directly with nanoscale substrate grooves. Cellular orientation (i.e. parallel

or perpendicular to grooves) was also found to be dependent on medium additives. This research is another example of how microtechnologies can be used to better define cellular responses and potentially provide more in vivo-like microenvironments. Christopher Chen and colleagues have used a range of microfabrication techniques to explore focal adhesion structures.[31, 32] By microprinting tiny islands of preferential adhesion areas, they found that FACs developed asymmetrically along adhesion islands and were able to explore FAC formation in response to stress.

In this context, we studied the advantage of circular microchannels over square microchannels in the cellular adhesion. Our results demonstrated a more successful adhesion, growth, and homogeneous distribution of the cells along the circular microchannel than those observed in the square microchannel used as a control.

**Cytotoxicity and biocompatibility.** Cytotoxicity and biocompatibility are relevant issues to any area of biology, but become particularly important when merging two fields, where common assumptions for either field might not hold

within the other.[13] Commonly used microfabrication materials and techniques must be reexamined to ensure compatibility with their biological inhabitant. High SAV ratios of microculture environments necessitate retesting the microculture biocompatibility of materials and sterilization methods (ethylene oxide, ionizing radiation, etc.) presently used in larger scale culture.[33, 34] Leaching from a container to a culture medium is a surface area-dependent process. As described earlier, the SAV can easily be an order of magnitude larger in microculture environments than traditional culture systems. This increased SAV means that an agent can leach into culture media 10 times faster in microculture than traditional systems. Even if the material is biocompatible, preparation steps such as gas steriliza-tion and ionizing radiation can leave leaching agents in plastic chamber materials. An amount of leaching that is tolerable in a large vat of cells might quickly become toxic in a microenvironment, especially considering the low doses necessary to cause cell damage.

## 1.4 Design principle

Microfluidic devices designed specifically for cell culture have certain requirements that distinguish them from microscale systems used for other applications in chemistry or physics. Design considerations of particular importance to microfluidic cell culture include: (1) the choice of material for device fabrication, (2) the geometry and dimensions of the culture region, and (3) the method of pumping and controlling fluid flow. The latter consideration ultimately dictates how the microfluidic device is connected to external components of the overall system. While it is clear that microfluidics offers the engineer—and the biologist—ultimate flexibility over system and experimental design given the plethora of options, it also implies that those involved with the experiment must be aware of all the available choices so that designs can be optimized according to the application. We highlight here the types of materials and options for control that have been largely accepted as the major classes within the microfluidics community, and discuss some of the new directions being pursued.

**Device materials and fabrication**. Similar to other niche areas within microfluidics, cell-based studies made the largest strides after the introduction of soft lithography. Soft lithography was popularized by Whitesides and his group at Harvard in the late 1990s, and comprises a set of fabrication techniques similar in concept to photolithography, but with significant benefits for biochemistry and biology.[35] The most popular material used in soft lithography is poly(dimethylsiloxane), or PDMS, a silicon-based elastomeric material with a number of physical and practical properties that make it desirable for experimentation. PDMS is fairly cheap and easy to mold, making it ideal for rapid prototyping of microfluidic designs and for transferring micropatterns with high fidelity via stamping techniques. PDMS is suitable for cell experiments because it is non-toxic to cells, is gas permeable, and has excellent optical properties, including low autofluorescence and optical transparency for imaging applications.[36] Furthermore, the elastomeric properties of PDMS allow it to readily deform when subjected to local displacements, allowing the integration of built-in valves and pumps via multilayer soft lithography. To make enclosed

microchannels, PDMS can be bonded to different materials (e.g., PDMS, glass, polystyrene) quite easily using various methods such as oxygen plasma treatment and additional curing.[37] While the many advantages of PDMS have established its well-known popularity among microfluidics researchers, a growing number of reports are beginning to reveal some unfavorable characteristics of PDMS that may limit its future use for microscale cell culture. Kim and co-workers alluded to these challenges in a previous review on microfluidic perfusion systems. [38] More recently, however, it has been revealed that PDMS further confounds cell culture results by sequestering small hydrophobic molecules such as estrogen, and by leaching out uncrosslinked oligomers from the PDMS bulk during culture, which then bind to cell membranes. Also, as cells are exposed to PDMS for longer durations, cell metabolism and proliferation are affected, possibly as a result of the presence of PDMS. This growing awareness of the potential artifacts and biases associated with PDMS is providing an impetus for the microfluidics community to consider other options for materials. The most logical choice for an alternative material for devices is polystyrene

because it is the most common plastic used for traditional cell culture-ware. Polystyrene microfluidic devices for cell culture applications have recently surfaced in the commercial market (e.g., Bellbrook Labs, Integrated BioDiagnostics), [39] illustrating that the industry has already recognized a need to conform to the needs of biologists who are accustomed to certain materials. In academic research laboratories, micromolding techniques for fabrication of thermoplastic microfluidic devices has also been well-documented. A recent report from the Takayama group has employed a hot embossing technique using epoxy molds to fabricate polystyrene-based microfluidic devices for cell culture, with potential to incorporate soft substrates such as polyurethane or PDMS as a bonded surface.[40] In yet another example, rapid prototyping of polystyrene microfluidic devices has been achieved by the use of "Shrinky-Dinks" thermoplastic sheets. Shrinky Dinks plastics are an arts and crafts toy for children with the property that drawn artwork on the plastic surface can be shrunk in size after heating the material. This property was recently exploited by Khine and co-workers to produce positive relief masters for microfluidic devices. Together, these

developments are revealing a trend toward microfluidic devices made with more common bioware materials, as well as a trend against further investments into materials with undesirable and unknown effects on cultured cells. For the foreseeable future, however, PDMS will continue to provide an affordable rapid prototyping option for most research laboratories, and will work in concert rather than in competition with other materials such as polystyrene.

**Geometries**—Lithographic techniques allow for infinite possibilities when it comes to geometry, but for cell culture applications, some important considerations must be recognized. First, microchannel dimensions for cell culture are typically at the larger end of the spectrum for channel sizes, ranging from 100 to 1000 microns. Smaller microchannel cross sections, on the order of tens of microns, are common in chemical applications such as electrophoretic separations, and are more suitable for single cell analyses or for chips designed for cell sorting and cell manipulation. These applications have been reviewed elsewhere. For biological experiments, unless single cell analysis is coupled with high throughput methods

for measuring endpoints, enough cells will need to be cultured in the microchannels to permit population-based analyses, and this implies a need for larger channel culture regions. The flexibility in geometry permits the generation of stable gradients in both soluble and surface-bound factors. This is particularly useful for controlling the cell microenvironment in chemotaxis studies (as well as durotaxis and haptotaxis studies) where spatial and temporal concentration gradients can induce cell responses such as migration. An important geometric consideration in microfluidic channels is the height-to-width aspect ratio, especially for PDMS-based devices. While the deformability of PDMS was beneficial for fabricating multilayer devices with built-in valves and pumps, the same property leads to undesirable sagging and bulging of microchannel walls when (1) the PDMS layer is thin, (2) pressure is substantial, and (3) maintaining channel cross-sectional shape is important for analysis, such as in shear flow experiments. This issue would be less important for devices made of stiffer materials, such as glass or polystyrene.

**Pumps and valves: going tubeless**—Within microfluidic cell culture devices, fluid volumes must be transported and displaced from region to region, using valves and pumps that are either externally connected to the device, or directly built into the system. Inlet and outlet ports of the system serve as points of interaction between the culture region and the external world.[35] The majority of systems employ external pumps (e.g., syringe pumps for nonrecirculatory flow, and peristaltic roller pumps for recirculatory flow) that can be hooked up to the access ports via tubing. This is the method of choice for perfusion systems that rely on constant fluid flow to replenish nutrients and remove waste products in a timely manner. Using multilayer soft lithography, it is possible to incorporate pneumatic valves into the system to produce fully automated, high-throughput culture systems. Such a system provides a concrete example of the many benefits associated with microfluidic cell culture. The major concerns with this type of system are the large number of connections required, the potential for leakages at those connections, the technical expertise necessary for proper operation, and the need for elastic materials that possess properties with some

confounding issues. An alternative method of fluid replacement, which has potential for widespread acceptance because of its simplicity and compatibility with existing techniques in biology, is passive pumping. First developed by the Beebe group in the early 2000s, passive pumping relies on the surface tension of different-sized droplets placed at the inlet and outlet ports to drive fluid from one port to the other. The difference in droplet volumes induces a differential pressure between ports that generates flow in the microchannel. The major advantage of passive pumping is that it can be performed without connecting to an external pump, eliminating the need for tubing and interconnections at the ports. Passive pumping can be performed simply by pipetting the appropriate volumes of droplets at the ports, and is therefore amenable to automated liquid handling systems that are commonly used in major biology research laboratories. The ability to do experiments with “tubeless” microfluidics is likely to attract an increasing number of biologists to the microscale techniques that are currently being developed. In fact, other researchers have recently begun to study the physical phenomena related to passive

pumping in their own microfluidic systems, demonstrating that the technique is receiving support. While passive pumping is an effective method for many applications, it is limited to low volume flows and low pressures. Steady continuous perfusion of microchannels is better achieved with external pumps, even though droplets can theoretically be pipetted continuously in a passive pump cycle that simultaneously adds droplets at the inlet while removing droplets at the outlet.

**Membranes**—Certain on-chip accessories can be incorporated into microfluidic devices to add extra functionality to the cell culture systems. Three-dimensional networks are achievable by incorporating commercially available track-etched membranes (polycarbonate or polyethylene terephthalate) into the device during fabrication.[5] The membrane serves as a semi-permeable barrier that separates microchannels on different horizontal planes, allowing communication only at locations where microchannels intersect. Several groups have begun using this geometry for cell-based studies. The most notable is the Takayama group, who has employed

membrane-PDMS devices to study lung epithelial cell rupture,[41] and more recently, the adhesion of cancer cells on a microfluidic endothelium. The usefulness of this arrangement lies in the in vivo-like organization of the endothelium into luminal and abluminal compartments separated by a membrane that mimics the basal lamina. Such compartmentalization is potentially useful for coculture studies that involve communication between endothelial cells and neighboring cells from the stromal or smooth muscle layers.

## 1.5 Shape effect of microchannel

The shape of microchannels is an important design variable to achieve the desired cell culture performance. Interestingly, microfluidics provides important advantages over classical systems for cell and tissue cultures by displaying microchannels and structures mimicking the physiological parameters of the *in vivo* model. For example, many researchers use circular microchannels with endothelial cells

to mimic microvasculature *in vitro* models to replicate cardiovascular flow conditions.[42, 43] Indeed, endothelial cells grown on the bottom of a square microchannel are subjected to a varying shear stress that influences their elongation, differentiation, and growth. Although rectangular cross-sections are functionally adequate for many purposes, certain applications would benefit from microchannels with circular/round cross-sections. For example, in-plane microchannels are useful for immobilizing many cells for pharmacologic testing, single-cell electroporation, and cell–cell communication. However, rectangular cross-sections (vs. circular/round cross-sections) form poor seals between a cell and a microchannel opening, requiring the application of large immobilization pressure that often undesirably causes cell lysis. Furthermore, circular microchannels are intuitively suitable for microfluidics-based cell electromechanical studies involving micropipette aspiration and patch clamping to achieve a satisfactory seal between the cell and the channel inlet. Studies involving endothelial cell culture inside microchannels as an in vitro model for microvasculature can also benefit from the use of circular microchannels to more

closely mimic blood vessels. Rectangular microchannels limit cell growth on the channel bottom by exposing the cells to a non-physiological geometry. Cells grown on the bottom of a rectangular channel experience a varying shear stress which influences their alignment and elongation, differentiation. Moreover, the use of circular microchannels reduces the flow stagnation phenomenon present at the edges of square microchannels due to the symmetrical duct velocity profiles. It is well accepted that the degree of shear stress imposed on luminal endothelial cells, which depends strongly on the geometry of the flow channel affects their differentiation state, alignment, elongation and tight-junction formation. For these reasons, the geometry of the channel should replicate as closely as possible to the geometry of in vivo microvessels because of its essential role in the formation and maturation of vessels. Another advantage of circular microchannels is that they do not exhibit the flow stagnation phenomenon present in the corners of rectangular microchannels due to the symmetric velocity profile. This stagnation zone in rectangular microchannels leads to dispersion of the analyte plug in separation processes, undesirably increasing the theoretical

plate number. Here we propose innovative low cost approach to change the microchannel geometry fabricated by a micromachining technology.

# 2 Microfabrication techniques

## 2.1 Polymer materials

Microfluidics — the science and technology of manipulating nanolitre volumes in microscale fluidic channels — has impacted a range of applications, including biological test, micro and nanoparticles synthesis, single-cell analysis and tissue engineering.[44,45] These requirements point toward polymers as highly attractive materials for microdevice fabrication. Polymers generally imply inexpensive and low-cost fabrication techniques available for both rapid prototyping and mass production.[46] Polymers also possess a wide range of physical, chemical, and surface properties, which allow for fine tailoring of the chip material to a specific use. The main parameter which has to be considered in this classification is the so-called glass transition temperature (Tg).

This parameter, which can be measured as a more or less distinct bend in the curve of the specific heat capacity versus temperature (a first-order phase transition), has its origin in the molecular behaviour of the polymer material. If a polymer gets heated up at a certain temperature the energy of motion of parts of the polymer chain becomes large enough to overcome intramolecular friction. At this point in the temperature curve, larger segments of the polymer chain can suddenly start to move quite freely, leading to a significant softening of the material. Below Tg, a polymer behaves very much like a rigid, solid amorphous glass; beyond Tg, the material becomes flexible and soft. Another relevant parameter for the practical use is the so-called heat distortion temperature (HDT). It is a more empirically determined parameter and represent the maximum temperature for structural use of the material; beyond the HDT, the polymer cannot be exposed to any mechanical stress as it would simply give way. The third temperature relevant for polymers is the decomposition temperature (TD), at which the polymer decomposes and the polymer chains are broken, changing the basic nature of the polymer. So according to the position of Tg

and the behaviour of the polymer, the following material classes can be defined:[47]

1. **Thermosets (duroplastic materials):** in these materials, which can be liquid or solid at room temperature (often called resins), the molecular polymer chains start to cross-link (a process called curing) if the polymer is heated up or is exposed to sufficiently high doses of light or other radiation, thereby generating a rather hard and inflexible three-dimensional molecular network. If the curing process has taken place once, the polymer remains stiff even if reheated, as the curing involves an irreversible chemical reaction. Thermosets can therefore not be reshaped once cured. If heated further, the polymer decomposes or burns instead of melting. Tg typically is rather high and close to the decomposition temperature (TD). Typical examples of thermoset polymers in microfabrication are the resist materials for lithography, for microfluidic applications especially the photoresist SU-8 (see

Photolithography). The photocurable resins for stereolithography also belong to this material class.

2. **Thermoplastic materials**: this type contains the technical polymers which can be structured using replication methods like injection molding or hot embossing. Thermoplastic materials show a distinct softening at Tg which makes them processable around this temperature and a rather large temperature difference between Tg and TD, allowing for a large process window. In thermoplastic materials, no curing takes place at elevated temperatures so the molded parts can be reshaped many times by reheating. Most polymer components in the macroworld consist of thermoplastic materials, so it is not surprising that a large variety of microfabrication methods have also been developed for this material class. Typical examples are poly(methyl methacrylate) (PMMA) and polycarbonate (PC), which were among the first materials used for polymer microfabrication. For microfluidics, the cycloolefin polymers and copolymers

(COP, COC) have attracted much attention in recent years owing to their favourable optical properties, moldability and low water uptake.

**3. Elastomers**: in elastomers, the molecular chains are longer than in the other cases and typically do not show a chemical interaction but are physically entangled. If an external force is acting on the polymer, the polymer chains disentangle and allow the polymer to stretch elastically (as a technical definition, an elastomer exhibits at least 200% elastic elongation), returning to its original shape immediately if the external force is withdrawn. Owing to their low cost and easy handling, elastomeric materials, namely poly(dimethylsiloxane) (PDMS), have become a primary material for the low-volume manufacturing of microfluidic devices. In addition, their permeability for oxygen and carbon dioxide make them well suited for cell-based systems. Novel materials are being developed to overcome some of the limitations of

PDMS, namely the swelling in the presence of some organic solvents.

## 2.2 Replication technologies

The enormous economic success of polymers in the macroscopic world is largely owing to the fact that low cost, high-volume fabrication methods exist. These methods are all based on the replication of a master structure (the geometrical inverse of the desired structure). Over the last 10 years, these replication methods have allowed large progress in the microfabrication field and built the foundation for the commercialization of microfluidic devices particularly in price-sensitive markets like the point-of-care (POC) diagnostic market. In terms of commercially applicable methods, hot embossing and injection molding play the major role, with microthermoforming being introduced recently. In the academic world, elastomer casting is the dominant method.[44]

## 2.3 Master fabrication

All replication methods have in common the need for a master structure (often also referred to as the replication tool, mold or mold insert). Although the requirements for such a master structure differ with respect to the physical parameters of the chosen replication method (e.g. force, temperature), four basic statements can be made: (a) the geometrical replication result can only be as good (or as bad) as the geometrical accuracy of the master, (b) for the ability to separate mold and molded part (demolding step), no undercuts in the structure itself can be allowed, (c) the surface roughness of the master should be as low as possible (ideally peak–valley values of below 100 nm), and (d) a suitable interface chemistry between master and substrate has to be chosen. In order to generate the master structure, principally all microfabrication methods are suited. The proper selection of the master fabrication technology is one of the crucial steps in the product development of commercial microfluidic devices, especially as there is no generic recipe for this selection.

### 2.3.1 Hot embossing

Hot embossing has established itself in the last 10 years as a widely used method for the fabrication of polymeric microstructures both in academia and in industry.[48] The reasons for this development are the comparatively simple process which simplifies the selection of process parameters, the comparatively low requirements for master structures, the large range of suitable materials and the availability of commercial instrumentation. The process itself consists of the following steps: (a) The polymer substrate (wafer or sheet material) is placed in the system and heated in vacuum to a temperature just above the glass transition temperature; (b) The master structure is also heated to the same (or slightly higher) temperature; (c) The master structure is pressed into the polymer substrate with a force of typically 500 N $cm^{-2}$ in the case of PMMA or PC, the force depending on design, material and master material; (d) Master and substrate are isothermally cooled to a temperature just below Tg and then separated (demolding).

### 2.3.2 Injection molding

By far the most widespread fabrication process for polymers in the macroworld is injection molding.[49] The polymer material is fed as pre-dried granules into the hopper. In the heated barrel, a screw transports the material towards the injection port of the molding tool. During this transport, the polymer melts and reaches the tool in liquid form with a melt temperature of the order of 200–350 °C depending on the polymer. It is now injected under high pressure (typically between 600 and 1,000 bar) into the mold which contains the microstructured mold insert. For microstructure replication, it has to be evacuated to achieve a good filling of the mold and to prevent the formation of air pockets. Depending on the surface-to-volume ratio of the structure, the mold can be kept at temperatures below the solidification temperature of the polymer (typically between 60 and 120 °C, so-called cold-cavity process) or, in the case of small injection volumes and high aspect ratio structures, has to be kept at temperatures above Tg and cooled together with the melt. The need for this so-called variotherm process drastically increases the cycle

time; therefore, in commercial applications one goal of the development of the microstructure is the moldability with a cold cavity process. Typical cycle times for a cold-cavity process are of the order of 30 s– 2 min; a variotherm process can take up to 5 min. After opening the mold, the molded part will be ejected. Normally, remains of the material from the injection port (so-called sprue) will still be connected to the part which has to be removed, either mechanically by cutting, sawing or breaking, or with a laser. The big advantages of injection molding are the ability to form three-dimensional objects, which, in the case of microfluidic devices, means e.g. the integration of fluidic interconnects or through-holes.

### 2.3.3 Casting

By far the most widely published polymer fabrication process is the casting of elastomeric material, also often referred to as soft lithography.[50] Over recent years, the basic casting process has been modified into a large variety of different variants (e.g. microcontact printing μCP, replica molding, microtransfer molding μTM, micromolding in capillaries MIMIC, solvent-

assisted micromolding) The success of this process family is mainly owing to the following properties: (a) process simplicity, (b) material properties, (c) cost, (d) advantageous surface chemistries and (e) replication accuracy.[51] The starting point is the preparation of the elastomer. The most often used materials, Sylgard 184® by Dow Corning, General Electric RTV 615 and Elastosil® by Wacker are two-component systems, where typically ten parts of the base elastomer are mixed with one part of the curing agent. The curing itself is an organometallic cross-linking reaction, where three-dimensional bonds are formed. The resulting elastomer is optically transparent (down to about 300 nm), electrically insulating and chemically inert. To prevent the formation of air bubbles during mixing and casting, it is advisable to thoroughly degass the mixture, e.g. in an exsiccator or a simple low vacuum system. Typical degassing times are of the order of 20 min. The mixture is then simply poured over the master (e.g. an etched silicon wafer in a glass beaker) and cured. The curing can take place at room temperature in about 48 h or at elevated temperatures, e.g. 30 min at 115 °C, with a typical process window in the range between 40 and 80

°C. Curing temperature and ratio of the curing agent determine the stiffness of the elastomer sheet which can thus be adjusted depending on the application. After curing, the elastomer sheet is simply peeled away from the master. For a better release, it is advisable to make the surface of the mold hydrophobic, e.g. by silanization. Reservoir holes can simply be punched into the cured material. Structured PDMS sheets can easily be bonded to a glass plate or another sheet of polymer owing to its excellent adhesion properties.

### 2.3.4 Micromachining methods

Micromilling is one of the oldest microfabrication techniques and to date one of the most used in many laboratories around the world (Fig. 4,5).[52, 53] Milling is a subtractive manufacturing process that uses rotating cutting tools to remove material from a starting stock piece, commonly referred to as the workpiece. The basic milling system, or mill, consists of (1) a worktable for positioning the workpiece, (2) a cutting tool (most commonly an endmill), and (3) an overhead spindle for

securing and rotating the cutting tool. Milling, which has origins dating back to 1818, has undergone significant advances, and now represents a major tool in a machinist's repertoire. The positions of the worktable (X and Y-axis) and spindle (Z-axis) are traditionally adjusted by hand with mechanical levers and cranks, but modern mills now employ computer numerical control (CNC) that automates the process, thereby improving repeatability and precision, reducing human error, and adding advanced capabilities (e.g., the direct conversion of computer-aided design (CAD) models to finished parts). Milling machines with CNC capability (i.e., CNC mills) are available with a wide range of technical specifications, encompassing varying levels of stage precision, spindle speeds, and automation. Modern CNC mills are versatile and capable of fabricating devices with features ranging in size from several microns to several meters. The wide availability of cutting tool shapes, materials, and sizes makes the mill amenable to fabricating many types of features in many different materials. Perhaps the most enabling aspect of using a CNC mill is the ability to fabricate a part directly from a three-dimensional (3D) CAD model, making it easier

and faster to convert design concepts to working prototypes. Latest advances in technical features have enabled improved precision and resolution down to the micron scale, leading to the use of the term micromilling to describe fabrication of increasingly more intricate parts with microscale resolution. Micromilling can be useful in microfluidics applications for two main functions: (1) machining the mold used in subsequent fabrication steps (e.g., embossing or injection molds) or (2) machining microchannels and features directly into the final part. In the latter case, micromilling offers a key advantage: a plastic workpiece can be milled into a device in less than 30 min (for simple designs), significantly reducing turnaround time from design to prototype. Milling is well characterized for producing large features in common machining materials such as steel and aluminum.

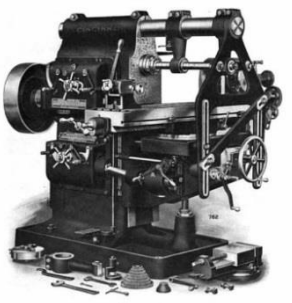

Fig. 4 Old version of micromilling machine


Fig. 5. Modern version of micromilling machine

## 2.4 Bonding

Regardless of the fabrication method employed, the sealing of the open microchannels is necessary to produce the final

enclosed fluidic paths, and thus a critical step in the fabrication process invariably involves bonding a capping layer to the microchannel substrate.[54] Depending on the functional requirements of the final microfluidic system, there are a number of considerations that must be taken into account when selecting and implementing an appropriate bonding method. Bond interfaces must provide suitable chemical or solvent compatibility to prevent degradation during use, without compromising dimensional control of the microchannels due to deformation during the bonding process. Other important considerations for the bond interface include surface chemistry, optical properties, and material compatibility and homogeneity of the channel sidewalls. Microfluidic bonding techniques may be categorized as either indirect or direct. Indirect bonding involves the use of an adhesive layer to seal two substrates and encapsulate microchannels fabricated in one or both of the substrates. In contrast, direct bonding methods mate the substrates without any additional materials added to the interface.[44]

- Adhesive bonding (Indirect bonding)
- Thermal fusion bonding (Direct bonding)
- Solvent bonding (Direct bonding)
- Surface treatment and modification (Direct bonding)

**Adhesive bonding**: Due to the simplicity of adhesive bonding, this approach has been widely used for sealing thermoplastic microfluidic chips. One of the simplest adhesive bonding techniques is the use of glues, i.e. liquid adhesives that set through the evaporation of solvent, or epoxies and acrylates that cure (polymerize and crosslink) after mixing with a catalyzing agent. This technique has been discussed as a viable approach to polymer microfluidic bonding, but there are few published examples where this strategy has been successfully employed, likely due to the challenge of channel clogging.[44, 55] More commonly, adhesive bonding is performed by applying a thin layer of a high viscosity liquid adhesive which forms a bond after curing by UV light irradiation. UV-curing adhesives are generally manufactured from synthetic resins containing photoinitiators to enhance resin crosslinking upon exposure to

specific wavelengths of light. While a wide range of UV-curable adhesives is available, they are most commonly derived from polyester or acrylate resins which possess a surface energy less than the critical wetting tension of most typical thermoplastics except olefin thermoplastics like COC and PS, thereby ensuring spontaneous wetting of the microfluidic chip surfaces.

**Thermal fusion bonding**: During direct thermal bonding, substrates are heated to a temperature near or above the Tg of one or both of the substrate materials, while applying a pressure to increase mating contact forces. The combined temperature and pressure can generate sufficient flow of polymer at the interface to achieve intimate contact, with inter diffusion of polymer chains between the surfaces leading to a strong bond. Under ideal conditions, the resulting bond strength can reach the cohesive strength of the bulk material. An important advantage of direct thermal bonding is that the microchannels possess homogeneous surface properties when identical materials are used for both the microchannel and capping substrates. This feature, together with the relatively

high bond strengths and overall simplicity of the approach, have made direct thermal bonding the most common method for sealing microfluidic chips. Thermal fusion bonding of various thermoplastics has been widely demonstrated, including PC and PMMA.[56, 57] One major challenge of thermal fusion bonding is channel deformation caused by un-optimized temperature and pressure. Thus, properly controlling temperature, pressure, and time is critical to achieve high bond strength while limiting deformation of the embedded microchannels due to bulk polymer flow.

**Solvent bonding:** A chemical acts as a solvent for another material when the molecules of each material do not exhibit a tendency to separate from one another, i.e. when the total molecular force of attraction between the dissimilar materials is greater than the force of attraction for each material alone[54]. For interactions between organic solvents and polymers, solubility can be adequately described by the Hildebrandt parameter (d), defined as the square root of the cohesive energy density for each molecular system. As evident from Table of figure 6 , appropriate solvents are available for

bonding a wide range of microfluidic thermoplastics. In practice, the majority of reported solvent bonding work for microfluidic applications has focused on PMMA. Solvent bonding of PMMA has been performed by simply immersing the chips in ethanol for 10 min before mating them together under pressure.[58] Because the solubility parameters of PMMA and ethanol are substantially different, the immersion process could be performed without significant channel deformation. Solvent bonding of PMMA chips has also been explored using either ethanol, methanol, or isopropanol, with the solvent applied to the capping layer by quickly dipping the polymer chip into a solvent bath. The chips were immediately removed and bonded to the microchannel plates using different pressures, temperatures, and times to determine optimum process conditions. The bond strength of optimum process exhibit as high as 23.5 MPa. Direct application of acetonitrile and a solvent system comprising an aqueous solution of dimethyl sulfoxide (DMSO) and methanol have also been reported for PMMA bonding. In the latter example, softening of the PMMA was shown to be limited to only the first 50 nm

of the surface following 30 min exposure to the solvent mixture.

**Surface treatment and modification:** increased surface energy serves to improve the wettability between mating surfaces, enabling more intimate contact and ultimately enhancing mechanical interlocking and interdiffusion of polymer chains between the surfaces. Higher surface energies can also improve bonding through the generation of electrostatic interactions, and surfaces possessing high specific energy in the form of polar functional groups can produce hydrogen or covalent bonds across the interface capable of providing bond strengths exceeding the cohesive strength of the bulk polymer. Surface treatments are widely used in macro-scale polymer engineering to increase surface energy prior to bonding. Examples include solvent or acid treatments, surface grafting, and both vacuum and atmospheric plasmas. For microfluidic applications, plasma activation is commonly used to modify PDMS surfaces with silanol groups, resulting in covalent bond between mating elastomer layers, and this technique has been widely applied to thermoplastic

microfluidics as well. Energetic ions, electrons, and UV photons in plasmas can possess sufficient energy to break chemical bonds on the target surface, producing highly reactive free radicals which assist in forming the desired charged surface groups and increasing the overall energy density of the surface. Plasma modification has been reported as a method for reducing processing temperatures and improving bond strength for microfluidic chips fabricated from a range of thermoplastics including PMMA, COC, PC, PS, and PET using both oxygen and ambient air plasmas (Fig. 6).

| Thermoplastic | $\delta$ [(J/cm$^3$)$^{1/2}$] |
|---|---|
| PTFE | 12.6 |
| PE | 16.3 |
| PP | 16.3 |
| COC | 17.7 |
| PMMA | 20.1 |
| PS | 18.7 |
| PVC | 19.4 |
| PC | 19.4 |
| PET | 21.8 |
| **Solvent** | **$\delta$ [(J/cm$^3$)$^{1/2}$]** |
| Cyclohexane | 16.7 |
| Methylene dichloride | 19.8 |
| Ethylene dichloride | 20.0 |
| Acetone | 20.4 |
| *n*-Hexanol | 21.8 |
| Isopropanol | 23.4 |
| Acetonitrile | 25.1 |
| Ethanol | 26.0 |
| Dimethyl sulfoxide | 26.7 |
| Methanol | 29.6 |
| Water | 47.7 |

Fig. 6. Fabrication materials and solvents for bonding process

# 3 In vitro blood-brain barrier models

## 3.1 Microfluidic-based model to study nanoparticle transport across the brain endothelium under flow conditions

The blood-brain barrier (BBB) with its distinctive tissue structure acts to separate the peripheral blood from the central nervous system (CNS), thereby maintaining brain homeostasis.[59, 60] Among others, the permeability of the BBB is controlled by the brain endothelial cells, that regulate the selective transport from the blood to the brain and vice versa.[61] The endothelial layer is also essential in preventing the entrance of toxic substances to the brain.[62] Indeed, due to this tight barrier, the majority of drugs fail to cross the BBB. Consequently, the blood brain barrier (BBB) represents a challenge in the development of new nano-delivery systems able to reach the central nervous system (CNS).[63] In order to test the efficacy of new nanocarriers, it is fundamental to use *in vitro* models that better resemble the *in vivo* cell culture

conditions.[64] In this part of the work, we demonstrate for the first time the ability of a membranotropic peptide, namely gH625, to transport a cargo across the BBB layer under flow conditions that mimic the blood flow rate. To this aim, a BBB microfluidic device was designed based on a transparent polyester porous membrane sandwiched between a top and a bottom overlying channel made of PMMA. Our data clearly indicate that this microfluidic system allows the growth of brain endothelial bEnd.3 cells and the formation of a confluent layer at 7 days of culture that hinders the passage of albumin and nanoparticles compared to blank porous filter. Very interestingly, the decoration with gH625 peptide enhances the adhesion of nanoparticles at the endothelial layer and the BBB crossing, thus suggesting the efficacy of gH625 as a delivery platform to the brain.

## 3.2 PMMA Microfluidic chip with a blood brain barrier

Nowadays, most BBB experiments are performed in static Transwell assays.[65] However, *in vivo* brain endothelial cells are subjected to the blood flow that lacks in the commonly used *in vitro* models. In this context, *in vivo* models are the best candidates to study the transport across the BBB. However, these models are scarce, expensive and are difficult to study both in detail and real-time. *Ex vivo* and *in vitro* models are good alternatives, as they are qualified for their simplicity and controlled environment. Moreover, shear stress derived from blood flow positively affects endothelial cell physiology and tight junction formation. Two microfluidic models of the BBB have recently been reported, demonstrating the feasibility of an organ-on-chip approach.[5, 66] Till now, there are only a few papers published of dynamic BBB models and in particular no works have investigated BBB crossing by NPs in flow conditions up to now to the best of our knowledge. The aim of this work has been to test the ability of gH625 peptide to transport nanoparticles across the brain endothelium under

flow conditions. Herein, for the first time we developed a microfluidic BBB model using polymethil metacrilate as fabrication material. PMMA, is advantageous due to its desirable material properties including optical transparency, low cost, cheap manufacturability, possibility of chemical treatment and biocompatibility. Many researchers use PMMA to fabricate microfluidic devices for cell culture and biological studies. [67] To mimic the blood flow in brain capillaries, we designed an *in vitro* μ-fluidic BBB model. The system was realized in such a way as to permit the growth of the cells on a porous filter up to reaching the confluence and to separate two compartments delimited by endothelial layer, namely the blood side and the brain side. The transendothelial electrical resistance (TEER) was measured and the indirect immunofluorescence against Claudin 5 was stained to analyze barrier tightness. The microfluidic chip contains a transparent polyester microporous membrane (Corning Costar, Cambridge, MA,USA) sandwiched between a top and a bottom overlying channel (Fig. 7). The endothelial layer is obtained on the porous membrane directly into the device after culturing mouse brain

endothelial cells. A collecting chamber is also integrated on the top channel in order to collect traversed NPs. To verify our issue, we first characterized the growth and the formation of a confluent brain endothelial layer of bEnd.3 cells within the *in vitro* µ-fluidic system through brightfield and confocal microscopy observations. Then, the permeability of this system was tested by using fluorescent albumin (BSA) as a standard molecule and amine-modified fluorescent polystyrene nanoparticles as a control indicating the functionality of our model. Finally, the capability of gH625-conjugated nanoparticles to adhere to and cross the brain endothelial layer under flow conditions were investigated.

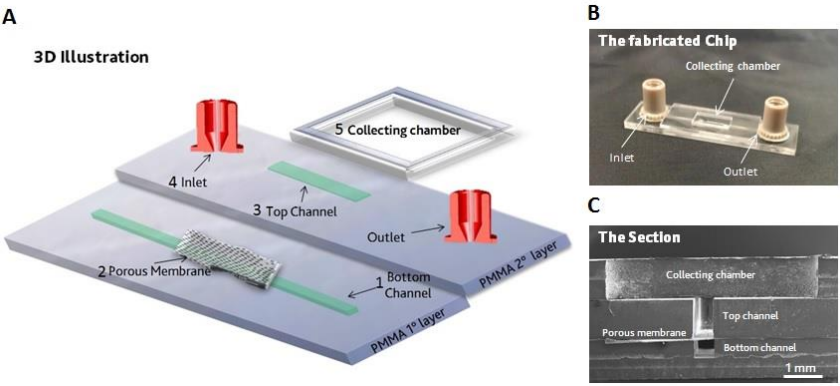


Fig. 7. 3D illustration, photograph and SEM image of the fabricated microfluidic chip. Scheme of the structure and design of the developed BBB microfluidic system (A), including (1) the bottom channel, (2) polycarbonate membrane, (3) the top channel, (4) the Nanoport UPCHURCH® connectors and (5) collecting chamber. Picture of the fabricated chip (B) and SEM image of a section of the device (C).

### 3.2.1 Design, electrodes integration and microfabrication of microfluidic system

In this section, we detail the design and fabrication of the microfluidic chip. It is based on different PMMA layers bonded via solvent evaporation. Specifically, the assembly of the PMMA layers was performed by simply immersing PMMA substrates in ethanol for 10 min. The immersed substrates

were immediately removed, aligned and clamped for an overlap of the top and bottom channel, after the heat treatment was initiated at 58 ° C for 45 minutes. Before proceeding with the assembly (Fig. 7) of the chip the manufacturing substrates was cleaned using a common soap (RBS Ditalclean, Brussels). The bonding between the top channel substrate and the bottom channel substrate allows to enclose the polyester membrane on which cells are grown afterwards. PMMA is a thermoplastic polymer that can be easily micromachined by micromilling (Minitech Machinery Corporation) which is a fast prototype technique. In addition to bond NanoPorts Upchurch® to PMMA microdevices, we developed a hybrid system, which glues commercial nanoports with an alternative biocompatible epoxy adhesive. The microfluidic chip shown in Figure 7 is composed of two PMMA channel substrates (12x50x1mm) and a PMMA collecting chamber (12x30x1mm). The depth and width of the channel is different onto the two PMMA substrates, 889 µm width and depth for the bottom channel and 1.2 mm of depth and 889 µm of width for the top channel. The microtool used to micromachine the PMMA was in all the cases a flute

endmill with an 889 µm in diameter. In the second PMMA layer we microfabricated inlet and outlet holes to connect the microfluidic chip with the classic fluidic equipment such as syringe pump and tubing. The fabrication process consisted of 4 steps: (1) preparation of the chip draft using Draftsight (Cad Software), (2) micromachining of PMMA layers; (3) ethanol-assisted bonding process and (4) bonding Nanoport Upchurch to PMMA substrate (Fig. 7-8). The certified positioning accuracy of the three-axis are 12”/300mm in x-axis, 9”/228mm in y-axis, and 9”/228 mm in z-axis. To standardize the fabrication process, the PMMA substrates used in this study were purchased from the same batch of the polymer supplier (GoodFellow Cambridge Limited, England).

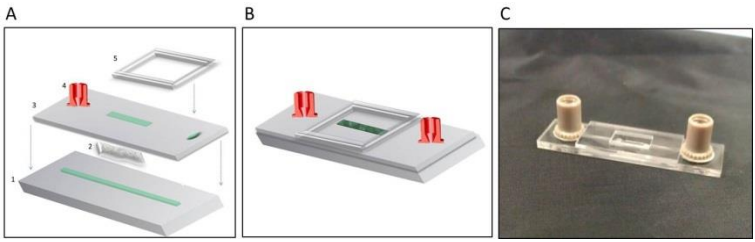


Fig. 8 Assembly of the PMMA microfluidic device.

**Surface characterization: SEM image and roughness profile**

To measure the roughness of the micromilled PMMA substrate with various cutting parameters (table in figure 9), a profilometer with a resolution of 0.01 µm was used (VEECO DEKTAK 150) (Fig. 9) and subsequently the same samples were characterized by SEM.

The microchannels dimensione were: 3 mm in length, 0.889 mm in width, and its depth 0.889 mm. To investigate the influence of various parameters like spindle speed (N)-feed rate (F), the micromilled surface quality of PMMA, multiple factor levels, listed in the Table 1, were used in the experiments.

| Cutting Parameter | Level 1 | Level 2 |
|---|---|---|
| N-Spindle speed r.p.m. | 10000 | 13000 |
| F-Feed rate (mm/min) | 15 | 30 |

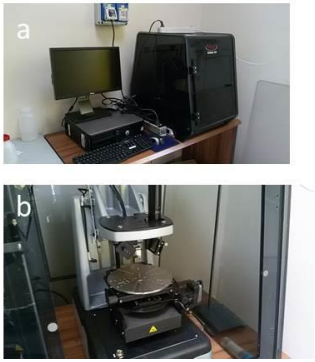


Fig. 9 Cutting parameters and profilometer instruments

After a set of preliminary experiments which led to the choice of factors indicated in table of figure 10, totally there were 12 reservoirs micromilled. To evaluate the surface quality after micromilling, SEM characterization was carried out and the surface roughness, Ra(µm) was measured with the VEECO DEKTAK profilometer. SEM images in Figure 10 show the surface characteristics based on the combinations of different cutting parameters listed in Table. All of the measured roughnesses are between 0,24 and 0,48 µm. At the same N value, when the feed per flute is reduced, reducing the feed rate, the channel roughness is always lower. As shown in Table o figure 10, the combination selected for an optimal channel micromachining is No 5, spindle speed 13000 and feed rate 15 mm/min, this result was confirmed thanks to Scanning Electron Microscopy Image, Figure 10 c-d represent the combination No 5 in table 2.

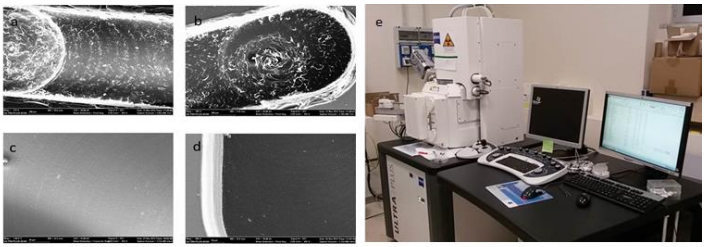


| No | N r.p.m. | F Mm/min | Ra (μm) |
|---|---|---|---|
| **1** | 10000 | 15 | 0,29 |
| **2** | 10000 | 30 | 0,37 |
| **3** | 10000 | 15 | 0,33 |
| **4** | 10000 | 30 | 0,4 |
| **5** | 10000 | 15 | 0,24 |
| **6** | 10000 | 30 | 0,38 |
| **7** | 13000 | 15 | 0,4 |
| **8** | 13000 | 30 | 0,45 |
| **9** | 13000 | 15 | 0,38 |
| **10** | 13000 | 30 | 0,47 |
| **11** | 13000 | 15 | 0,39 |
| **12** | 13000 | 30 | 0,48 |

Fig. 10. Sem images of micromilled PMMA substrate using different cutter parameter

## Alignment accuracy measurement

To characterize the accuracy and precision of the alignment into assembled devices, optical images of the chips were captured by a bright field stereomicroscope (IX71, Olympus Microscope) (Fig. 11). Alignment between the top and bottom layers was estimated by analyzing the microscopic images, including linear errors. To measure the linear errors (in the x and y directions), imaging software, ImageJ (Ver. 1.44p,

National Institutes of Health, USA), was exploited typically used for the image analysis. The linear errors, x and y, were measured at the intersection point of the designed cross pattern along the x- and y axes, respectively. The errors were indeed exploited to estimate the misalignment at the center area of the device. In order to quantitatively evaluate the level of accuracy of the PMMA ethanol-assisted alignment upon bonding, the maximum and minimum linear errors through the entire device were calculated.

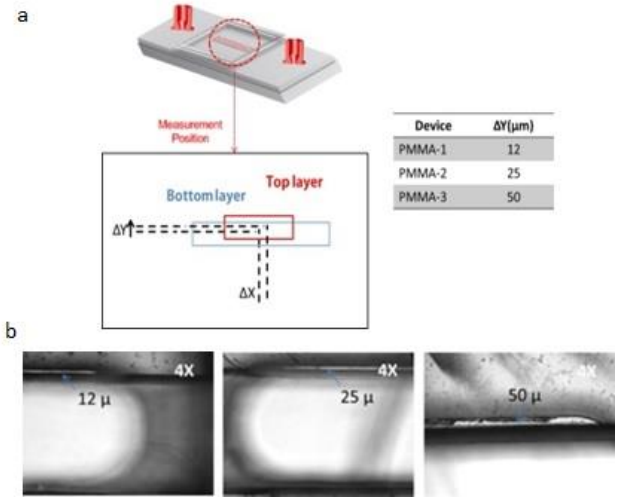


| Device | ΔY(µm) |
|---|---|
| PMMA-1 | 12 |
| PMMA-2 | 25 |
| PMMA-3 | 50 |

Fig. 11. Alignment accuracy measurement between two overlying microchannels

The results showed that for the irreversible chips with 10 µm thick membranes under the microscope using the cross patterns located at the center of the devices, the absolute ΔY misalignement error at the center can be estimated of around 12-50 µm.

### 3.2.2 Cell seeding, culture and barrier characterization

Mouse cerebral endothelial cells, bEnd.3 cells (American Type Culture Collection, Manassas, VA) were grown in DMEM with 4.5 g/L glucose, 10% Fetal Bovine Serum (FBS), 3.7 g/L sodium bicarbonate, and 4 mM glutamine, 1% non-essential amminoacids, 100 U/ml penicillin and 0.1 mg/ml streptomycin in 100 mm diameter cell culture dish, in a humidified atmosphere at 37 °C and 5% CO2. Cells used in all experiments were at passage 11–18. The fabricated chip was previously sterilized with 10% Penicillin-Streptomycin solution for 24 h at 4°C to prevent contamination. bEnd.3 cells were seeded at a density of $25 \times 10^3$ cells/$cm^2$ into microfluidic channel and the system was upside down, in order to allow cell adhesion to the polyester filter located on the top of the channel. Non-

adhered cells were removed 24 h after seeding by twice washing with fresh cell culture medium. Afterward, cells were allowed to grow until 7 days within the device. Medium was refreshed every 3 days. Cell growth was monitored over time by TEER measurement, phase contrast and confocal microscopy at 1, 3, 5 and 7 days of culture. In order to further verify cell growth in the microfluidic system, bEnd3 were fixed within system with 4% paraformaldehyde for 10 min at room temperature (RT) and stained with DAPI, hence, the number of nuclei was count by imageJ software 1.44p (Fig. 12).

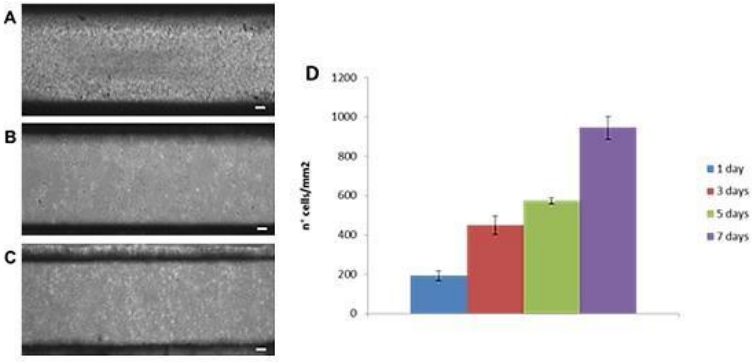


Fig. 12. Phase contrast microscopy pictures of endothelial cell layer in the PMMA microfluidic device**;** after 1 (A), 3 (B) and 7 (C) days from cell seeding. Bar 100 µm. (D) Cell density over culture time.

**Cell staining:** bEnd.3 cells were seeded in the channel and allowed to adhere to the membrane for 24 h at 37 °C. Afterward, the system was upside down, the channel was rinsed with fresh medium to remove non-adhered cells and incubated at 37 °C for 1, 3 and 7 days of culture. During cell culture TEER was monitored using the electrodes system described in next section. The results reported in figure 14 C shows a TEER increase achieving a plateau value. Figure 12 shows phase contrast images of bEnd.3 cell layer after different days of growth in the microfluidic device. As reported, cell confluency increased over time. After 7 d post cell seeding, the cells had formed a confluent monolayer as demonstrated by the nuclei and microfilament fluorescent staining. Image analyses confirmed that the cell density per area increased over time. To verify the formation of tight junctions, indirect immunofluorescence against Claudin 5 was performed at the $7^{th}$ day of culture. Confocal microscopy images show that bEnd.3 cells were able to express Claudin 5 protein, prevalently localized around the cell boundaries thus indicating the formation of tight junctions. These data demonstrate the capability of the microfluidic device to allow

the growth and the correct formation of the confluent brain endothelial layer. The presence of tight junctions was determined by immune-staining with anti-Claudin 5 antibody (Life Technologies). Briefly, bEnd.3 cells were fixed with 4% paraformaldehyde for 10 minutes. After permeabilization with 0.1% Triton-X100, cells were incubated with the blocking buffer (BB) (0.5% BSA in PBS) and were stained with the anti-Claudin 5 primary antibody for 1 h at RT. Then, the Alexa-488 anti-Mouse secondary antibody diluted in BB was incubated 1 h at RT. In order to detect actin filaments, TRITC-Phalloidin (Sigma) was used. After fixation and permeabilization, bEnd.3 cells were incubated for 30 minutes at RT. For nuclei staining DAPI (Sigma) was used. All samples were then observed at confocal microscope (Leica TCS SP5 MP) with a 25× water-immersion objective (Fig. 13).

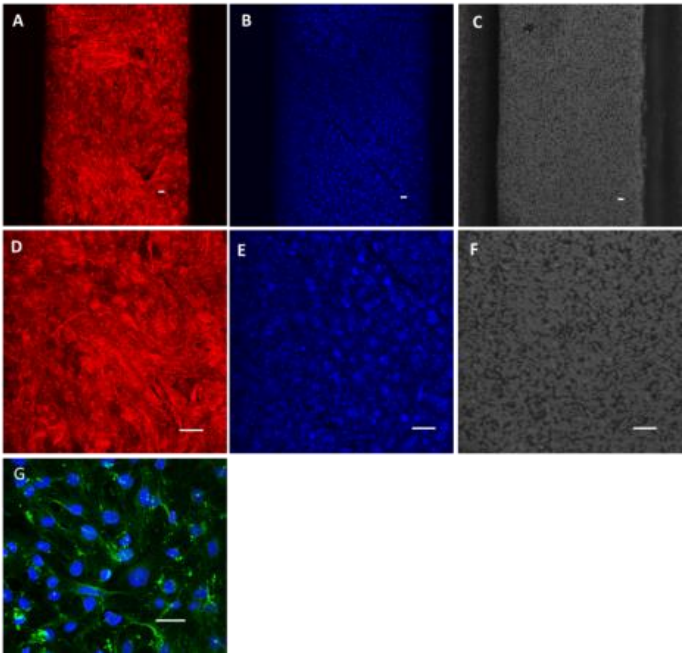


Fig. 13. 7-day growth confluent bEnd3 cell layer. (A, D) Phalloidin (red) staining of cytoskeleton; (B, E) DAPI (blue) staining nuclei; (C, F) Brightfield images of the polyester filter. (A-C) Images acquisition performed with a 10 x dry objective. (D-F) Zoomed images shown in panels (A-C). (G) Claudin 5 (green) and DAPI (blue) staining of tight junctions and nuclei, respectively, acquired with a 25 × water-immersion objective. Bar 50 µm.

***Electrodes integration and TEER measurement:*** TEER measurements were carried out by connecting the BBB chip to an AUTOLAB PGSTAT302N (potentiostat/galvanostat)

equipped with a FRA32M module (frequency response analysis module). Impedance spectra were recorded in potentiostatic mode with an amplitude of 0.01V and frequencies ranging from 100kHz to 0.1Hz between two Pt electrodes. Pt electrodes were realized by sputtering deposition of 20 nm of platinum on the surface of metallic microfluidic tips with a final diameter of 1.3 mm (Fig. 14 A). For each measurement 3 readings and 50 data points (logarithmic frequency step) per reading were collected. The least-square optimization method was used to fit the measured impedance data to an electrical equivalent circuit model, reported in fig. 14 B. In the adopted model the constant phase element represents the dual layer capacitance of Pt electrodes (CPEdl), which is in series with the resistance of the medium (Rmedium) and the cell monolayer, which is denoted as the resistance of cell (Rteer) and the capacitance of the cell membrane (Ccl) in parallel. Porous polymeric membrane was used as supporting material for cells adhesion and growing. This membrane represents an additional resistive term (Rmem) which is in parallel with Rteer. Thus, for each impedance spectra an apparent Rteer (Req) was

collected and then corrected (eq. 1) for the membrane resistance to obtain the effective Rteer.

$$Rteer=(Req*Rmem)/(Req-Rmem) \qquad \text{eq. 1}$$

Rteer was normalized for the cross sectional surface area of the chip (0.054 $cm^2$) to calculate TEER value in $Ohm*cm^2$.

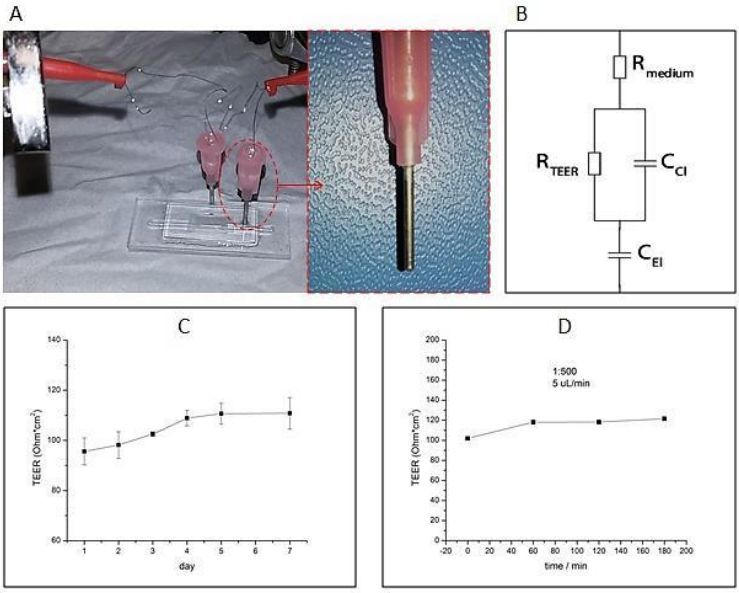


Fig. 14. Electrodes integration (A),model (B) and TEER results to establish tight junction formation (C) and tight junction preservation upon flushing (D).

### 3.2.3 BSA and nanoparticle transport across the BBB

In order to further validate the BBB microfluidic device, we performed transcytosis experiments to test the capability of BSA to cross the endothelial layer. BSA is known to cross the BBB through adsorptive transcytosis, therefore it can be used as a valid standard to measure the system functionality under flow conditions. BSA transport experiments were performed after 7 days of cell culture under static conditions. The device was connected to a syringe pump and the cells were subjected to a flow rate of 5 µl/min comparable to others reported in literature shows the percentage of BSA transported mass across the system at regular time points. In absence of cells, almost 100% of BSA was transported by 30 minutes. Conversely, in the case of microfluidic system with the confluent cell layer, there was a significant decrease in the BSA permeation, even at 30 min, with about 16 % of transported BSA after 3 h under flow conditions. Also for aminated polystyrene NPs, we observed a significant reduction of the transport in presence of the endothelial cell layer compared to the filter alone. In particular, after 3 h

under flow conditions, only 2.72 % of NPs were transported across the filter in the presence of the cell layer respect to 13.45 % of transported NPs in the case of the filter alone. These results indicate that the presence of the layer hinders the passage of solutes and nanoparticles across the filter thus validating our system (Fig. 14).

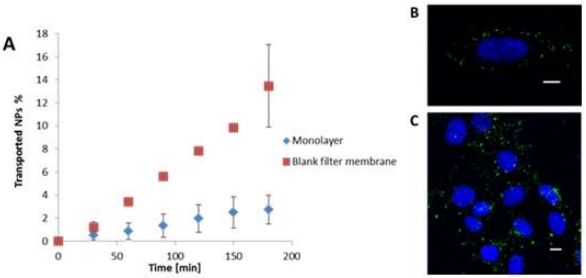


Fig. 15. Percentages of transported blank NPs under flow conditions (Flow rate: 5 µl/min), in absence and in presence of the confluent cell layer. Bar: 10 µm.

***Nanoparticles and conjugation to gH625 peptide:*** The conjugation of gH625 to amine-modified fluorescent polystyrene nanoparticles was performed as described previously. Briefly, the peptide was preactivated with EDC (1-Ethyl-3(3-dimethylamino-propyl)-carbodiimide, ydrochloride) and NHS (N-Hydroxysuccinimide) in molar ratio of 4:4:1 in PBS buffer at pH 7.4, at room temperature (RT) under stirring for

30 min. NPs were conjugated with the preactivated-peptide, in MES 0.1 M buffer at pH 5.5 for 3 h at RT in presence of Tween 20 and the yield of the reaction was higher than 90%. The peptide-NPs were purified from the un-conjugated-NPs by exclusion chromatography on a 1 × 18 cm Sephadex G-50 (Amersham Biosciences) column. The fluorescence spectra of peptide-NPs and un-conjugated NPs were measured in a Cary Eclipse Varian fluorescence spectrophotometer.

***Transport assay*** Transport experiments across the BBB microfluidic system were performed at the 7th day after seeding. Briefly, a 5 ml syringe was loaded with a FITC-BSA solution at the final concentration of 0.1 mg/ml in cell culture medium supplemented with 40 mM HEPES buffer. For nanoparticle transport experiments, the sysringe was loaded with blank and gH625-NP suspensions in buffered cell culture medium at the final concentration of $9.20 \times 10^{10}$ NP/ml. The syringe was then allocated on a syringe pump (Harvard Apparatus Pump 11 Elite) connected to the inlet of the microfluidic system by a tube (Radel Tubing 1/16x020xsoft). The outlet of the system was connected to an Eppendorf

through the same kind of tube in order to collect the output flow media. The collection chamber was filled with 90 µl of cell culture medium. The experiments were carried out in a plexiglass incubator at 37°C and solutions are flowed at 5 µl/min flow rate. Compounds and NPs that crossing the endothelial monolayer are collected in the apical chamber. Experiments were carried out for 3 h, drawing the medium in the collection chamber every 30 minutes and replacing it with fresh medium. The transport of BSA and nanoparticles across the BBB layer was estimated by fluorescence measurements. Through a spectrofluorometer (Perkin-Elmer, USA). Data were reported as percentage of transported BSA and NPs compared to the initial concentrations of the fluorescent compounds (Fig. 15). After the “transport assay” experiment we tested the integrity of the cell layer by measuring the TEER, the results reported in figure 14 D did not show any decrement of the TEER confirming that the layer is not damaged.

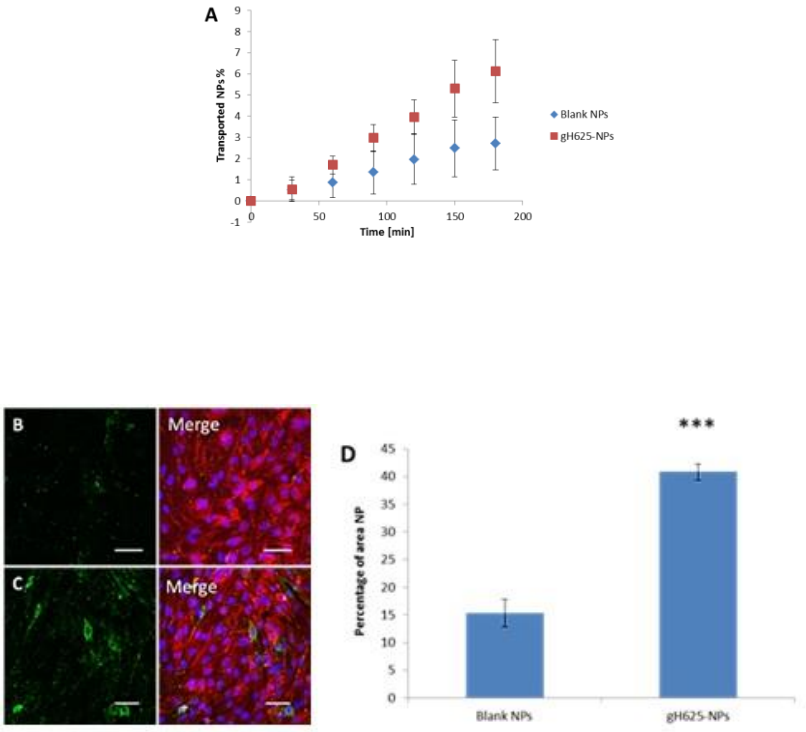


Fig. 16. Blank and gH625-NPs (A) transported under dynamic conditions (Flow rate: 5 µl/min). Confocal images of the confluent cell layer in the µ-fluidic system, after experiment: B) blank NPs, C) gH625-NPs (green) and phalloidin (red) staining of cytoskeleton. Bar 50 µm. D) Percentages of blank and gH625-NPs per area. The data are presented as the mean ± SD (n = 5), *** $P < 0.0001$.

***Image analysis:*** In order to quantify the amount of NPs in the cells, after the NP transport experiment under flow conditions, bEnd3 cells were fixed in the microfluidic system and stained with DAPI. Five images for each sample were acquired by confocal microscope and analyzed. The quantification of fluorescent NPs was performed by using area calculator plugins of ImageJ software as follow: color image was split in two different channel, green (NPs) and blue (nuclei). Hence, the percentages of fluorescent areas were normalized for the number of nuclei. Results were expressed as mean ± standard deviation (SD). Statistical analyses were performed using a one-way analysis of variance (ANOVA). Results repeats were compared by analysis of variance (ANOVA), and a $p$ value < 0.05 was considered statistically significant (Fig. 15).

## 3.3 PMMA Modular and reusable microfluidic chip with a brain endothelium layer

### 3.3.1 Introduction

Microfluidic technologies provide important advantages over classical methods for cell and tissue culture by displaying structures and networks at relevant physiological length scales, and by incorporating forces that bring the cell-based assays a step closer to mimicking the in vivo model.[68] In addition, microfluidic devices possess several advantages, such as low fabrication cost, low chemical consumption, small footprint and better control in both spatial and temporal domains. Therefore, they have been broadly utilized for chemical, biological and medical applications. Two main applications in biomedicine are the use as in vitro model of the blood–brain barrier (BBB), and as model for extravasation of tumor cells from one side and NCs from the other side across physiological barriers. In both cases, the fabrication process includes the design and assembly of a microfluidic chip that recreates in vitro the endothelial membrane.[69]

Mimicking the functional properties of this complex tissue interfacing the brain with the systemic vascular environment is critical for the development of novel NCs drugs and is an extremely challenging task. With the recent development of microfabrication methods and microfluidic technology, microfluidic systems are gradually being used as robust cell-culture tools for various cell-based assays. NCs for tumor solid therapy is advantageous over conventional medicine for the potential to enable the target delivery of encapsulated drugs to cancers owing to the enhanced permeability and retention (EPR) effect. The development of microfluidic strategies for NCs crossing solid tumors is useful in selecting NCs with higher chance of success from a large pool of nanoparticle formulation, and eliminating those that would otherwise have failed in clinical studies with many animals. In addition, up to now the mechanisms of in vivo tumor cell motility are still unclear, while thanks to microfluidics it could be possible to measure spatially resolved endothelial permeability and show particular pathways in endothelial barrier impairment. The most favorable benefit of using microfluidics for biology research is the ability to control the local cellular

microenvironment precisely without (or with less) interference from the external environment. In recent years Kim at all have developed a PDMS microfluidic device as an in vitro model of the blood brain barrier that mimics the dynamic cerebrovascular environment with fluid shear stress and the results indicate that the model express sufficient key characteristic of a BBB model. Griep at colleagues have recently developed a similar microfluidic models of the BBB;[66] the chip made in PDMS consists of two microfluidic channels separated by a conventional polycarbonate membrane. These devices present the main drawback of not being modular, so membrane cannot be recovered. Other groups have developed screw systems for microfluidic chip bonding, which, behind the strong hold, are complex to manage and not easy to guaranty a good alignment of the channels while tightening the screws.[70] [71]Here, we present a simple, fast and low cost procedure to fabricate a reusable microfluidic chip in a hybrid configuration which presents a temporary bonding. Finally, an endothelial cell layer was formed by culturing brain endothelial bEnd.3 cells inside the proposed microdevices.

### 3.3.2 Design and microfabrication of microfluidic system

The magnetic system developed in this work ensures a strong hold, great simplicity in bonding and debonding operations which is crucial to avoid invasive manipulation for cells and finally it guaranties an optimal alignment. The latter is also due to the use of a rigid material like poly(methyl methacrylate) (PMMA) which allows no leakages under liquid pressure even though most of the area is not clamped by the magnets. Among various materials, PMMA, is also advantageous due to its desirable material properties including optical transparency, low cost, cheap manufacturability, possibility of chemical treatment and biocompatibility. We have designed and developed this chip with removable bonding for two improvements: to observe directly the membrane drawing it through a fast procedure and to deconstruct the system for inspection and washings. To validate our modular microfluidic device we used cell imaging, directly on the membrane to observe structure and morphology which was possible thanks to the proposed method. In this section, we detail the design and fabrication of

a modular microfluidic chip based on magnetic removable bonding for study of transendothelial passage. The PMMA microfluidic chip may be used in two different ways: the cell culture can be performed directly on the membrane assembled in the chip, or externally in Petri dish and placed before the assembly, thanks to presence of magnets that guarantee a strong bonding between bottom and top layer with no need for invasive bonding based on oxygen plasma or organic solvents. The modular microfluidic chip consists of a top chamber and bottom channel connected via a transparent polyester microporous membrane (Corning Costar, Cambridge, MA, USA) with uncoated porous inserts (pore size 3.0 μm). The top chamber contains a bottom channel to perfuse the apical surface of the cells. The bottom channel acts as a reservoir for transport across the cell layer and provides support for the membrane. For a better characterization, we fabricated an innovative and reusable modular system with aligned grooves to insert neodymium magnets (Magnets4you, Lohr a Main, Deutschland) for a removable and mechanically robust bonding.

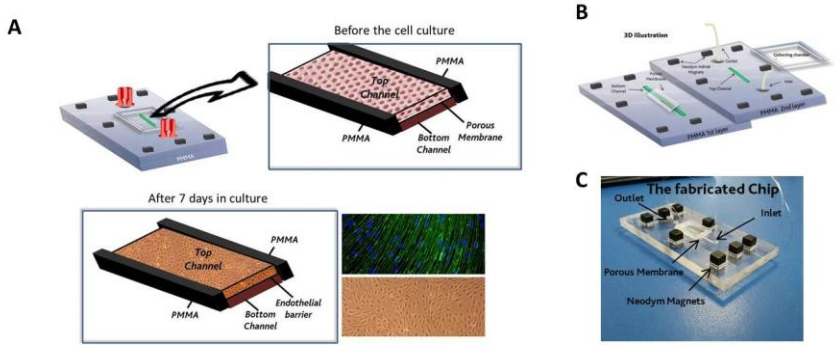


Fig. 17. Structure and design of the modular and reusable BBB microfluidic system. (A)The modular microfluidic chip consists of top and bottom channels connected via a transparent polyester microporous membrane. (B)(C) The 3D illustration and fully fabricated PMMA microfluidic chip, The depth and width of the channel are different on the two PMMA substrate.

This design of the microfluidic device provides an instrumented platform with fast removable bonding to study various epithelial cell transport processes. The microfluidic chip shown in figure 16 is composed of a two PMMA channel substrates (40x78x2mm) and a PMMA collecting chamber (10x18x2mm). The depth and width of the channel are different on the two PMMA substrates, 889 µm of depth and 889 µm of width for the bottom channel and 1.2 mm of depth

and 889 µm of width for the top channel; the assembled chip houses two overlying crossing channels to control dynamic experimental setup, a polyester membrane between two PMMA substrates that is located at the channel junction with an area of 6 $mm^2$. In the PMMA layers we fabricated sites to insert Neodymium magnets having a special epoxy coating for the use in extreme conditions of humidity. Indeed, previous magnets with no coating determined a toxicity effect on cultured cells. In order to achieve precise alignment and strong removable bonding across the entire device, the chip was designed with neodymium magnets placed in the PMMA substrates according to the design to assure the positional accuracy. To assure a perfect strong bonding, to pump liquid in the channel, we have fabricated a PDMS membrane on the first PMMA layer. In the chip, the magnets embedded in the two different PMMA layers will be arranged with the opposite poles facing each other to promote the attraction force for the bonding. The process consists of five steps: (1) micromachining of channels and magnets sites; (2) deposition of a PDMS membrane with thin thickness on first PMMA layer; (3) insertion of the polyester membrane between the two

layers of PMMA and magnets on their sites; (4) magnets_assisted bonding process and (5) bonding Nanoport Upchurch to PMMA substrate developed in a previous work. The microfluidic chip was fabricated by sequentially micromachining PMMA layers by using a micromilling machine (Minitech Machinery Corporation), which has five major components including a micromilling spindle. The advantages of using micromilling for polymer microfluidic devices include faster fabrication process, lower cost, easier user interface, and being capable of fabricating complicated structures, rapidly prototyping polymer microfluidic devices for research idea testing and validation. The certified positioning accuracy of the three-axis are 12" / 300mm in x-axis, 9" / 228mm in y-axis, and 9" / 228mm in z-axis. To minimize the experimental uncertainty, the PMMA substrates used in this study were purchased from the same batch of the polymer supplier (PMMA, substrate thickness 2 mm, Goodfellow). To design a draft of the microfluidic device we have created a schematic of our chip using Draftsight (Cad Software). The microtool used in the microfabrication process was 2-flute endmill with different diameter of 889 µm and 2,38 mm (Performance

Micro tool). In the first layer a 30 mm length bottom channel was fabricated using an end mill the dimension were about 889µm x 889 µm (width x depth). The top channel was about 889 µm x 1.2 mm (width x depth) and overlying to the bottom channel. Before proceeding with the assembly of the chip a PDMS layer was deposited on the PMMA top substrate.

### 3.3.3 Cell culture and preliminary results

Mouse cerebral endothelial cells, bEnd.3 cells (American Type Culture Collection, Manassas, VA) were grown in DMEM with 4.5 g/L glucose, 10% Fetal Bovine Serum (FBS), 3.7 g/L sodium bicarbonate, and 4 mM glutamine, 1% non-essential amminoacids, 100 U/ml penicillin and 0.1 mg/ml streptomycin in 100 mm diameter cell culture dish, in a humidified atmosphere at 37 °C and 5% CO2. After confluency, the cells were trypsinized with 0.25 % trypsin and 0.05 % EDTA (Gibco, Invitrogen, USA) for 3 min, and then concentrated by centrifugation and resuspended with the complete medium to adjust the cell concentration to 2 × 105 cell/mL. The hybrid PMMA-PDMS microchannel (diameter of 800 µm) was

sterilized with 10% Penicillin-Streptomycin solution in PBS for 24 h at 4°C. We used a magnets coated with an epoxy biocompatible material to preserve from oxidation. The surface of the microchannel was incubated with DMEM + 10% FBS at room temperature (RT) for 1 h. After washing with Dulbecco's phosphate-buffered saline (DPBS; Gibco, Invitrogen, USA), the harvested cells were seeded onto the microchannel. After 60 min incubation in a humidified 5 % CO2 incubator at 37 °C for cell attachment, the chip was immersed in a Petri dish containing a static media solution and cells were allowed to growth up to 7 d. The proposed modular system guarantees the possibility to re-open the microchannel for a better characterization. In order to further verify cell attachment and growth in the system, bEnd.3 cells were fixed within the system with 4% paraformaldehyde for 10 min at RT and stained with DAPI (Sigma) and TRITC-WGA (Invitrogen). All samples were then observed at confocal microscope (Leica TCS SP5 MP) with a 25× water-immersion objective (Fig.17).

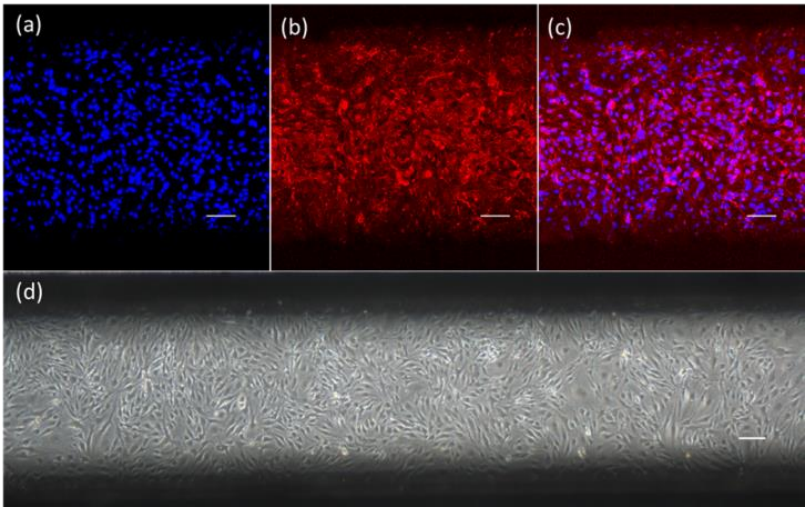


Fig. 18. Confocal images of bEnd3 cells after 7 days of culture in the modular microfluidic device. DAPI (blue) staining nuclei (a); WGA (red) staining of cell membranes (b); merge image (c). Phase contrast microscopy images of endothelial cell layer in the microchannel (d). Scale bar 100 µm.

# 4 In vitro microvessel models

## 4.1 From square to circular polymeric microchannels by spin coating technology: a low cost platform for endothelial cell culture

### 4.1.1 Introduction

Microfluidics is a micro-technological field that deals with the handling of fluids and dispersions of nano and micro-objects.[72, 73] Interestingly, microfluidics provides important advantages over classical systems for cell and tissue cultures by displaying microchannels and structures that can mimic the physiological parameters of *in vivo* models.[2, 68] Many researchers use circular microchannels with endothelial cells to replicate cardiovascular flow conditions in *in vitro* models.[10, 43, 74] The advantage of circular microchannels over square microchannels in mimicking blood vessels for endothelial cell culture has also been recently demonstrated by an MIT research group that developed a rapid casting of patterned vascular networks for perfusable engineered three-

dimensional tissues.[75] The use of circular microchannels reduces the flow stagnation phenomenon present at the edges of square microchannels due to the symmetrical duct velocity profiles.[42] Conversely, endothelial cells grown on the bottom of a square microchannel are subjected to a varying shear stress that influences their elongation, differentiation, and growth.[76] Together with the strong use in microvascular capillary field, the use of circular microchannels is convenient in the preparation of cylindrical or round microparticles, as well as circular fibers and cell-laden hydrogels and to control microparticle migration.[77, 78] Recently, open microchannels have also been used for cell growth or to flux fluids by capillary effect without using pump systems. Both applications may benefit from a circular microchannel shape as in the case of closed microchannels. Various methods to fabricate polymeric microchannels have been reported depending on the end goal of industrial mass production or rapid prototyping at the research laboratory level, including photolithography coupled with wet etching, reactive ion etching, stamp based techniques, such as soft lithography, hot embossing and injection molding, as well as ablating

technologies like conventional machining, laser ablation and finally direct 3D printing.[38, 79] Direct 3D printing can easily produce rounded microchannels, but with some limitations in the resolution, while more complex techniques -such as wet etching or reactive ion etching- can be tuned to produce rounded and smaller microchannels. During the last decade several research groups have developed new techniques for the fabrication of circular microchannels. For example, recently Abdelgawad et al. *et al.* presented an innovative approach to fabricate circular microchannels from square geometry using a pressurized air stream inside PDMS-filled microchannels.[80] This technique lacks the ability to create branches, while curved structures and long circular channels may be not uniform. Alternatively, mechanical micromachining techniques, such as micromilling, proved to be an effective approach to fabricate complex 3D micro-scale features on metals and polymers. However, microchannels obtained by micromilling technology exhibit a high roughness profile, while in many applications a very smooth surface is required. Recently, by exploiting the surface tension phenomenon, it has been demonstrated that microlenses can

be obtained by spinning liquid PDMS on square microstructures, fabricated by photolithography.[9, 81] In 2012, De Ville and co-workers used the surface tension of alginic acid sodium salt solution inside square microchannels, so that such liquid creates rounded protrusions;[82] it is a simple and low-cost method for the fabrication of round PDMS microfluidic channels but it lacks the capability to easily tune curvature; no circular microchannels could in fact be obtained. To the best of our knowledge, an easy, low cost and versatile method to fabricate circular microchannels is therefore still missing. In this paper, we present an innovative fabrication method that combines spin coating and micromilled square microchannels to fabricate circular microchannels ensuring easy and low cost manufacturing that can be applied without the need for clean room facilities (Fig.18).

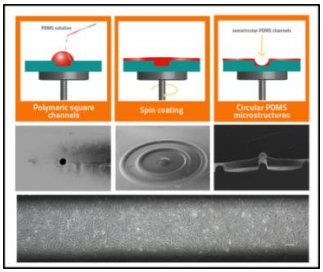


Fig. 19 General idea to fabricate circular microchannels from square geometry

In this process centrifugal forces and surface tension cause together the localization of the liquid PDMS in the corners of the channel providing the desired curvature. We demonstrate that -by tuning parameters such as viscosity, geometry of the starting square channel, spin coating speed- it is possible to obtain circular and, more in general, round-shape and closed microchannels. The geometry and quality of the semi-circular PDMS channels created by spin coating technology was characterized using optical microscopy, scanning electron microscopy (SEM) and a surface profilometer, while AFM was used to characterize channel roughness. The versatility of this method was further demonstrated by proving the possibility to produce hybrid solutions and rounded microchannels different from circular ones. Finally, preliminary experiments

on brain endothelial bEnd.3 cells indicate the capability of the circular microchannels to allow a good adhesion, an improved growth and a more homogeneous distribution of the cells over the surface of the channel than those obtained with the square microchannel of comparable size used as a control.

### 4.1.2 Square microchannels fabrication

**Materials and equipment:** The poly(methyl methacrylate) PMMA substrates used in this study, thickness 1.2 mm, were purchased from Goodfellow Cambridge Ltd, (UK) and belong to the same batch of supplied PMMA substrates. PMMA offers several material properties including optical transparency, low cost, inexpensive manufacturability, possibility of chemical treatment and biocompatibility. A PDMS prepolymer and a curing agent (Sylgard 184 elastomer kit) were purchased from Dow Corning Corporation (USA). Hexane puriss. p.a. was obtained from Sigma-Aldrich, (USA). The microtools used in the microfabrication process were 5 tr series 2 flute micro square end mills with different diameters:

800, 400, 200, 100 and 50 µm and 1 tr series 2 flute micro ball end mill with a diameter of 800 µm; they were purchased from Performance Micro tool (USA). Micromilling machine was purchased from Minitech Machinery Corporation (USA). Syringe pump 11 Helite Series was purchased from Harvard apparatus (USA). Fabricated microchannels were inspected by electron scanning microscopy (SEM) (Ultraplus Zeiss) and profilometer (Veeco Dektat 150). For the spin coating process, a spin coater from Laurell (WS-650 Series) was used. Mouse cerebral endothelial cells, bEnd.3 cells, were purchased from American Type Culture Collection, Manassas, VA. Dulbecco's Modified Eagle's Medium (DMEM) with high glucose, trypsin, Dulbecco's phosphate-buffered saline (DPBS), fetal bovine serum (FBS), penicillin and streptomycin were purchased from Gibco Invitrogen, USA. Sodium pyruvate and DAPI were purchased from Sigma-Aldrich, (USA). Glutamine was purchased from Lonza Group Ltd,Basel, Switzerland. Non-essential amino acids were purchased from EuroClone S.p.A., Milano, Italia. Red fluorescent WGA and Alexa488-phalloidin were from Gibco Invitrogen, USA.

The square microchannels were typically fabricated by sequentially micromachining PMMA layers by using the above mentioned micromilling machine. Milling is a subtractive microfabricating process that uses rotating cutting tools to remove material from a substrate. To standardize the fabrication process of semi-circular microchannels from square geometry, we micromilled microchannels with different width-depth: 800-400, 400-200, 200-100, 100-50 and 50-25 µm. Different ratios of width-depth, such as 800-300 and 400-100 µm, were also used to show capability of tuning the curvature of the final rounded microchannels. Moreover, to show the versatility of this method -by using a 400 µm end mill- we micromilled microchannels with branches that emulate arterioles and venules, as well as ring-shape microchannels. To design a draft of the microstructures we created a layout by Draftsight (Cad Software). During micromilling, spindle speed, feed speed and plunge rate per pass were set to 10 000 rpm, 15 mm $s^{-1}$, and 20, respectively.

### 4.1.3 Spin coating and fabrication of circular PDMS microchannels

Spin coating is a common technology for the production of polymer films of controlled and uniform thickness. To create semi-circular microchannels of different diameters from square microchannels we used the above mentioned spin coater. A typical process involved depositing a small PDMS droplet, mixed in ratio 10:1 with curing agent, (around 1 ml) at different degrees of dilution with hexane onto the center of a substrate and then spinning at high speed (2000 rpm for 20 s). PDMS precursor was previously exposed to vacuum to eliminate air bubbles for at least 30 min. The PMMA-PDMS with round open microchannels was baked in the oven (1 h, 75 °C), to finalize the PDMS curing process. PDMS solution was poured on the hybrid PMMA-PDMS master and cured at 80 °C for 2 h. Particularly, in order to prevent adhesion of the PDMS replicas on the master, this was treated with oxygen plasma to activate the surface using a plasma chamber (Plasma prep II, SPI) for 1 min at a pressure of 0.3 mbar and power of 37 W, immersed for about 2 min into a silane solution (i.e., a mixture

of 94% v/v isopropanol (Sigma Aldrich), 1% acetic acid (Sigma Aldrich), 1% Fluorolink S10 (Solvay), and 4% deionized water and then placed in an oven at 75 °C for 1 h, thus allowing a complete reaction of the master surface with the fluorinated polymer. After curing, the PDMS was peeled off from the PMMA-PDMS master. The entire procedure was repeated to prepare final PDMS open microchannels. In the case of closed microchannels, two symmetric semi-circular microchannels were optically aligned and bonded through oxygen plasma activation of the surface. For the very small microchannels the alignment was aided by the use of two parallel motorized stages coupled with an optical camera. Temporary bonding was also carried out by using magnets with the advantage of obtaining high precision alignment avoiding motorized stages and the possibility to reopen closed microchannels after use.

### 4.1.4 Brain endothelial cell seeding and growth within square and circular microchannels

The fabricated open microchannels (400/200 µm width-depth), were bonded to a glass slide through oxygen plasma activation; closed microchannels were sterilized with 10 % penicillin-streptomycin solution in PBS before cell seeding for 24 h at 4 °C to prevent contamination. Both square and circular microchannels were coated with 10 µg/ml fibronectin (Sigma-Aldrich) for 1 h at 37 °C. Afterwards, the microchannels were washed with PBS to remove fibronectin excess. bEnd.3 cell suspension, at a density of $6 \times 10^5$ cells/ml, were injected into the channels. After incubation for 20 min in a 5 % humidified $CO_2$ incubator at 37 °C for cell attachment, bEnd.3 were reseeded within microchannels and incubated again, rotating the devices by 90° as previously described. This step was repeated three more times to cover the entire surface of the circular and square microchannels. Then, cells were allowed to grow for 24 and 72 h within the channels. At these time points, cells were fixed with paraformaldehyde 4% for 10 min and actin microfilaments and nuclei were stained with

Alexa488-phalloidin (Molecular Probes) and DAPI (Sigma). Samples were observed and images were acquired by multiphoton confocal microscope (Leica TCS SP5 MP) equipped with a 20 × dry objective. Z-sectioning images were acquired with 1.28 µm z-slice thickness. Cell density was calculated normalizing the number of nuclei for the area of the channels by Image J analysis software.

### 4.1.5 Results, characterization and validation

Motivated by the strong need in the microfluidic fields for circular microchannels, we propose an innovative hybrid technique that combines mechanical micromachining and spin coating process which is easy, reproducible and cost-effective. The process used to fabricate semi-circular microchannels is schematically outlined in figure 19. In particular, a mixture of PDMS precursor and curing agent is dispensed on the square microchannel obtained by micromilling followed by the spin coating process.

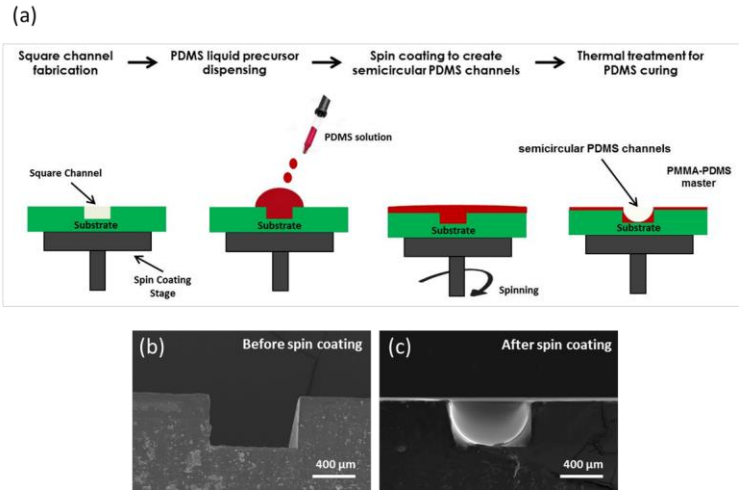


Fig. 20. Scheme of the spin coating process (a). Picture of a 800 x 400 µm PMMA microchannel before and after spin coating, respectively (b and c). The PDMS adhering to the microchannel wall after spin coating and consolidation by thermal curing.

The deposited liquid layer under spin coating is able to form a stable rounded PDMS layer on the walls of the square microchannel. Such rounded microchannel can be consolidated by curing the PDMS. Using undiluted PDMS solution, a PDMS circular shape in the square microchannel 800 x 400 µm was observed at around 2000 rpm and 20 s. In particular, fig. 19 displays the PDMS adhering to the microchannel wall after spin coating and thermal curing.

Undiluted PDMS proved too viscous to obtain a circular section in the case of narrower microchannels, independently of the spinning conditions; we used a mixture of PDMS and hexane at a ratio optimized according to each microchannel size in order to lower viscosity. The table in figure 20 reports the degrees of dilutions capable to provide circular shapes at 2000 rpm and 20 s of spin coating in the differently sized microchannels and the corresponding viscosities. In particular, the smaller the microchannels, the lower the viscosity used.

| Solution | Viscosity Pa s | Channel diameter µm |
|---|---|---|
| Undiluted PDMS | 5.86 | 800 |
| 3:1 PDMS : Hexane | 0.225 | 400 |
| 1:1 PDMS : Hexane | 0.043 | 200 |
| 1:3 PDMS : Hexane | 0.0057 | 50-100 |

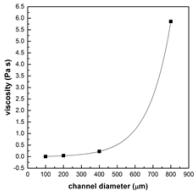


Fig. 21. Viscosity of the different PDMS solutions and corresponding circular microchannel diameters , measured using a Modular Compact Rheometer (Anton Paar).

From this table and related graph, it is possible to appreciate that reducing the size of the microchannels, dilution is less and less influent such that a semi-circular microchannel of 50 µm could be obtained with the same degree of dilution as the 100

µm microchannel. All the semi-circular shapes observed by SEM are summarized in Fig. 21. From the SEM micrographs it is possible to note the possibility to scale down the method in terms of microchannel size to around 50 µm. Circular shapes are evident from the SEM cross-section of closed microchannels (Fig. 21 i-n). In order to better characterize the uniformity of the microchannels along their extension and the reproducibility of the process, PDMS replicas made directly from the PMMA-PDMS masters (800/400 µm width/depth) were measured by using a profilometer. For the profilometer characterization we used a map scan type on hills profile, a stylus type radius of 2.5 µm and a measurement range of 525 µm. Other studies have investigated the use of spin coating technology to fabricate ultrathin and hyper-elastic PDMS nano-membranes with various thicknesses and sizes by using PDMS diluted with hexane. Herein, for the first time we have applied the thinning property of the PDMS-hexane mixture for scaling down, below 800 µm, the manufacturing of circular microchannels starting from cost-effective square PMMA microchannels.

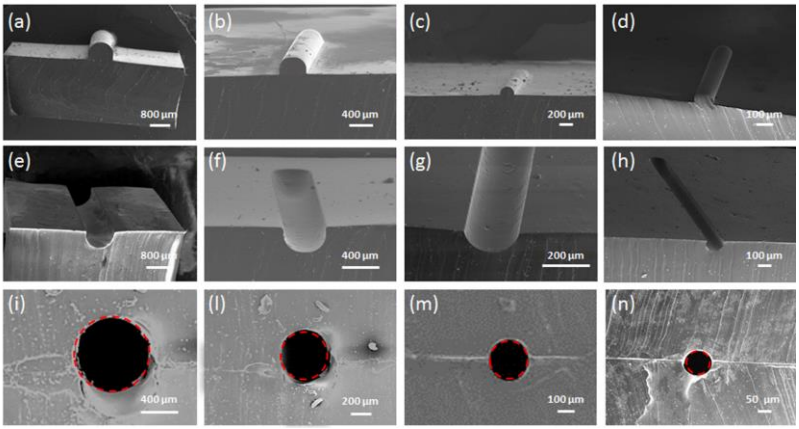


Fig. 22. SEM images of prepared round microchannels , semi-circular PDMS positive relief replicas (a-d), the corresponding semi-circular PDMS microchannels (e-h) and cross-section of bonded circular microchannels (i-n). The microchannels have diameters of 800, 400, 200 and 100 µm, respectively.

Circular microchannels can also be fabricated by micromachining a substrate with tapered angle ball tips. We made a comparison between surfaces obtained with our method and with direct channel fabrication by micromilling. From the optical microscope images, it was possible to observe the absence of the engraving lines in the case of the mold prepared with our method with an increase of the transparency (Fig. 22). Moreover, roughness profiles were characterized by AFM showing an enhancement of the

smoothness since it was ~ 228 nm compared to ~ 6 nm. This huge reduction in terms of roughness is highly desirable in microfluidics as previously mentioned and it is also advantageous from an optical standpoint since the final microchannel results much more transparent and internally inspectable.

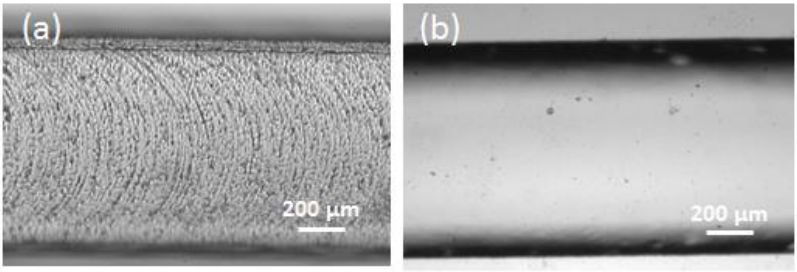


Fig. 23. Comparison in terms of roughness surface. A bright field microscopy image of semi-circular PDMS microchannels, replicated directly from a micromilled round microchannel (a) and from a semi-circular microchannel obtained using the proposed method (b).

To produce closed microchannels, after fabricating the two symmetric semi-circular microchannels we treated their surface by oxygen plasma so that they could irreversibly be bonded after alignment. They are examples of closed microchannels of very different sizes ranging from 800 to 100 µm. For the small microchannels the alignment was carried

out by using motorized stages coupled with an optical camera. As anticipated in the introduction, our method can also allow the fabrication of a hybrid PMMA-PDMS device where two symmetric PMMA-PDMS semi-circular microchannels obtained after PDMS spin coating on square microchannels in PMMA can be directly bonded, instead of acting as masters. In this case, by using small magnets embedded into the PMMA substrates it is possible to easily align even the smallest microchannels (down to 50 μm), avoiding motorized stages. With a hybrid device it is possible to combine the rigidity of the PMMA useful in the handling of the device -for example during the alignment step- with the softness and the low roughness of the spin coated PDMS. In addition, the PDMS layer in the case of magnetic bonding provides a strong sealing making temporary bonding with no leakage. PDMS is also useful as an optimal interface for cell cultures. A recently proposed method to fabricate circular microchannels is based on the use of compressed air injected in a square microchannel filled with PDMS precursor. Despite the advantage to avoid any alignment, air pressurized technology cannot be applied to branched microchannels. Moreover, the

gradient pressure inside the microchannel may prevent a uniform thickness of the PDMS around the wall, especially in the case of microchannels curved in plane. Our technique, instead, allows preparing branched microchannels as shown in Fig. 23 b, useful to emulate arterioles and venules with the same principle of single microchannels and microchannels curved in plane as shown with ring-shape microchannels in Fig. 23 c.

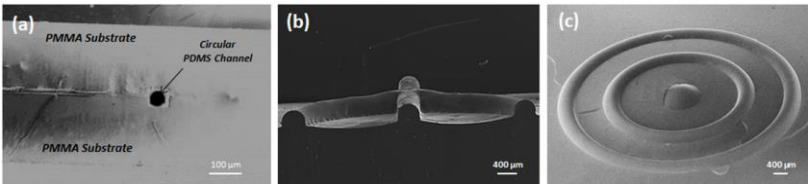


Fig. 24. Versatility of the spin coating process. A hybrid modular device made of PMMA and PDMS with neodymium magnets, a microchannel section SEM image (a). Branched and curved semi-circular PDMS microchannels, emulating arterioles and venules (b). A ring-shape microchannel obtained from a square geometry (c).

In addition, with the proposed method all the structures can be inspected before bonding thanks to the starting open microchannels and the vertical curvature of the final microchannel can be tuned. In particular, as described in the

experimental section, to obtain semi-circular shapes we used in all cases a width twice long as the depth of the square microchannel, while to tune the curvature of the final microchannel we were able to vary the depth of the square microchannel. Another recent work is based on the filling of square microchannels exploiting surface tension, which creates protruding round liquid to be replicated after consolidation. Although it does not involve expensive equipment for the fabrication, it is limited in the tuning of the curvature and in the production of discrete microchannels because of filling issues; therefore, circular microchannels were not obtained. In terms of flexibility other parameters that can be exploited with our method for the tuning of the curvature are viscosity (especially in the case of large widths) and spin coating speed. Moreover, we preliminarily tested the potential applicability of the as-prepared circular microchannels to sustain growth and formation of a confluent endothelium in vitro. To this aim, brain endothelial bEnd.3 cells were seeded inside a 400 μm-diameter circular microchannel and cultured for 24 and 72 h. We chose to work with brain endothelial cells as a model of endothelial tissue

and, in particular, of the blood brain barrier that currently represents one of the main goals of many therapeutic strategies and biomedical applications. As shown in Fig. 25, bEnd.3 cells were able to adhere and grow into the circular microchannels. In particular, after 72 h of culture, cells formed a confluent and very homogeneous monolayer that resembled the endothelial tissue. Conversely, when cultured into a 400 µm wide square microchannel, cell adhesion, spreading and proliferation were less efficient. More interestingly, the distribution of the cells along the square microchannel was not homogeneous. In particular, we observed a high cell adhesion in the middle of the channel and a poor adhesion in the corners. These observations were more evident at a longer culture time (72 h) and were in agreement with previously reported results. We quantified the cell density over time in both microchannel shapes. As shown in Fig. 24, this analysis shows a higher cell number per $mm^2$ in the circular microchannel compared to the square microchannel. Taken altogether, these data demonstrate the advantage of our circular microchannels in culturing endothelial cells compared to channels with squared geometry and their

potential use as scaffolds able to promote the formation of brain capillary-like structures.

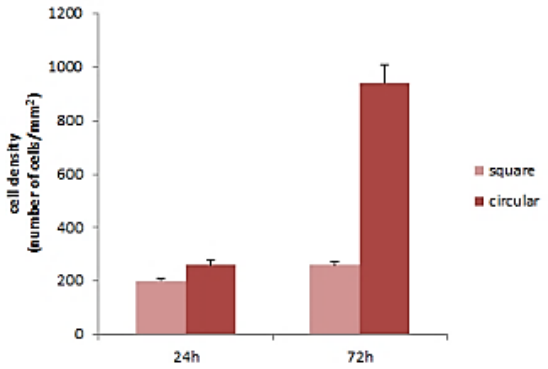


Fig. 25. Analysis of cell density in the square and circular microchannels

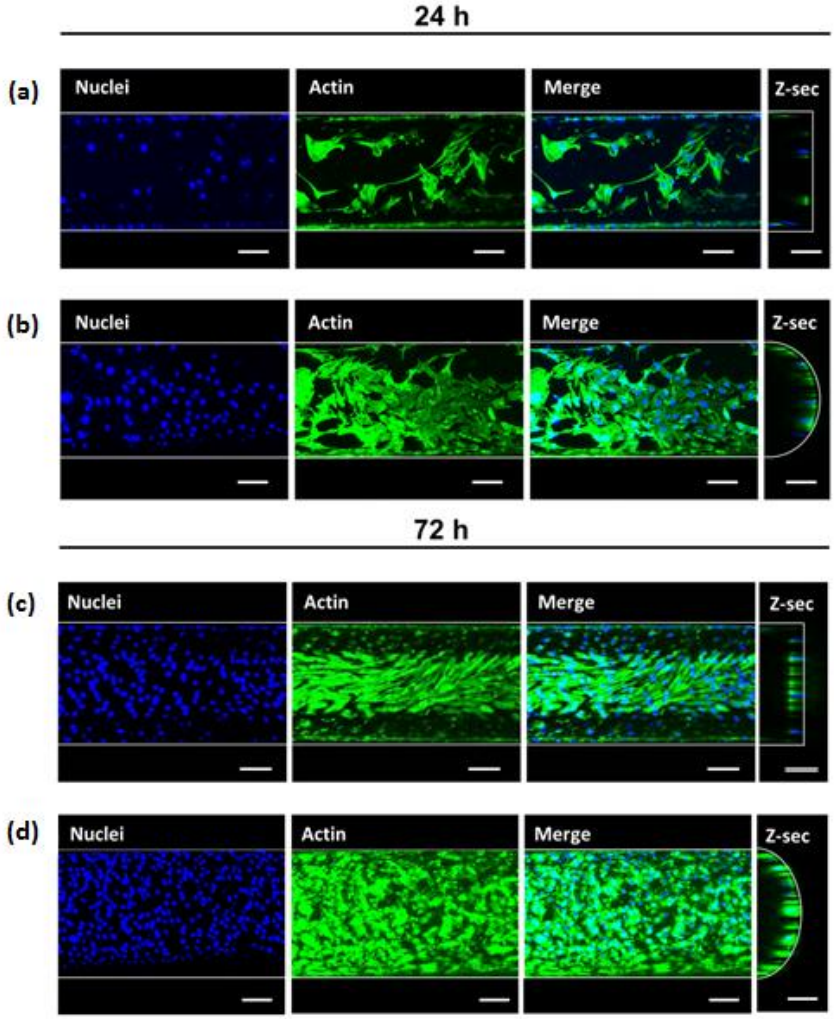


Fig. 26 bEnd.3 cell growth in square and circular microchannels

## 4.2 Confined gelatin dehydration as viable route to go beyond micromilling resolution and miniaturize biological assays.

### 4.2.1 Introduction

Microfabrication of polymer microfluidic chips is of growing interest in several application fields, from chemical processing to biotechnology, pharmaceutics and food manufacturing because of the benefits offered by miniaturized platforms.[44, 46, 83] In the last decade many research groups have investigated integrated micro-systems, the so called micro-total-analysis-systems (μ-TAS) and lab-on-chip (LOC).[1, 68] There is a strong need for microfluidic channels less deep than 50 μm in several fields such as synthesis, diagnostics and biology.[84] For example, Hwang and co-workers used a 16 μm deep microchannel to synthesize non-spherical magnetic hydrogel microparticles.[85] Bousse and colleagues developed a microfabricated analytical device on a glass chip (13 μm deep and 36 μm wide channel) that performs a protein sizing assay.[86] In the "organ on a chip" field, very small

microchannels are used to emulate microcapillary systems.[87] Small microchannels are useful in microfluidics for high-throughput screening applications, as the screening station from Caliper Life Sciences.[88] In addition, recently, many research groups have developed microfluidics platforms for manipulating and analyzing single cells owing to their ability to confine cells within microstructures having comparable dimensions to those of the cells.[89, 90] Photolitography has been widely exploited in the production of fluidic systems with controlled features at the microscale but it requires costly and complex equipment.[91] Alternatively, some works on shrinking approaches to scale down the size of microstructures have been recently reported.[39, 92, 93] For example, Focaroli et al. described a shrinking approach based on the agarose shrinkage of the lateral size corresponding to the width of the microchannel with no modulation of the depth.[92] Lal Das et al. described a method that provides a tridimensional size reduction by successive miniaturization through the shrinkage of hydrogels.[93] In principle the latter method could be exploited for the reduction of microchannel depths; however, 3D shrinkage typically promotes global deformation. To the

best of our knowledge, no strategy to provide a controlled shrinkage of microchannel depths has so far been proposed. Micromilling is a time-efficient and low-cost manufacturing method for the preparation of polymeric microfluidic devices.[53] One relevant limitation of micromilling is the inability to scale the microstructure depths down to a few microns.[94] In addition, already under 50 μm the reproducibility of the micromilling process is quite low, as described in the Results and discussion section. Therefore, the need for an easy, effective, reproducible fabrication technology of micrometric channel depths, not requiring complex and costly equipment, is still unfulfilled. To this aim, in this paper, we present the confined gelatin dehydration method that combines micromilling, as low cost equipment, with hydrogel dehydration in a laterally confined bowl to reduce the initial depth of microchannels ensuring the preservation of the final device planarity (Fig. 26). We compared tens of micron-sized microchannels (e.g. 20 μm) with same sized microchannels directly fabricated by micromilling and analyzed capability to scale down the depth to few microns by modulating initial PMMA microchannel depth and hydrogel concentration.

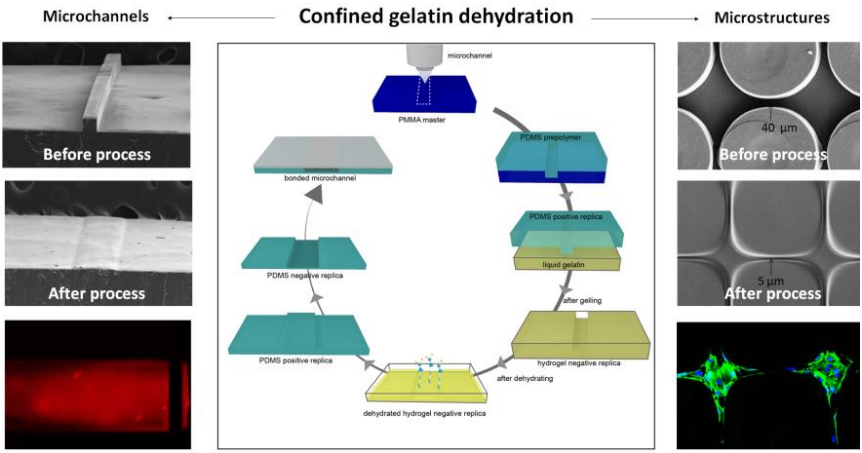


Fig. 27 The confined gelatin dehydration

We also adapted the proposed confined gelatin dehydration to a designed array of pillars to scale down (to 5 µm) the width of miniaturized channels interconnecting chambers. In order to demonstrate the efficacy of our method, the fabricated microfluidic channels were tested in terms of leakage by letting flow a red fluorescent liquid inside bonded device; no leakage occurred. In addition, we tested peculiar patterns characterized by arrays of areas interconnected by miniaturized microchannels -obtained with the proposed

method- for confined cell culture. The geometry and quality of the PDMS microchannel fabricated by dehydration process were characterized using optical microscopy and scanning electron microscopy (SEM), while a profilometer was used to characterize microchannel depth and roughness.

### 4.2.2 Fabrication methodology

***Materials and equipment:*** The PMMA substrates used in this study, thickness 1.2 mm, were purchased from Goodfellow Cambridge Ltd, (UK) and belonged to the same batch of supplied PMMA substrates. PDMS prepolymer and curing agent (Sylgard 184 elastomer kit) were purchased from Dow Corning Corporation (USA). Silwet L77 was purchased from Helena Chemical Company, Collierville, (USA). Gelatin, from porcine skin type A was obtained from Sigma-Aldrich, (USA). The microtools used in the microfabrication process were 3-flute endmills with different diameters: 380, 250 and 100 µm purchased from Performance Micro tool, (USA). Sulforhodamine B sodium salt was obtained from Sigma-

Aldrich, (USA). Tubing Silikon Peroxid/60 Shore ID 0.75 mm were obtained from IDEX Health & Science Gmbh (USA). Hypo Needles 18 AWG were purchased from Warner Instruments (USA). Vacucenter VC20/50 were obtained from Salvislab (Switzerland). Micromilling machine was purchased from Minitech Machinery Corporation (USA). Syringe pump 11 Helite Series was purchased from Harvard apparatus (USA). Fabricated microchannels were inspected by electron scanning microscopy (SEM) (Ultraplus Zeiss) and profilometer (Veeco Dektak 150). Mouse cerebral endothelial cells, bEnd.3 cells, were purchased from American Type Culture Collection, Manassas, VA. Dulbecco's Modified Eagle's Medium (DMEM) with high glucose, trypsin, Dulbecco's phosphate-buffered saline (DPBS), fetal bovine serum (FBS), penicillin and streptomycin were purchased from Gibco Invitrogen, USA. Sodium pyruvate and DAPI were purchased from Sigma-Aldrich, (USA). Glutamine was purchased from Lonza Group Ltd,Basel, Switzerland. Non-essential amino acids were purchased from EuroClone S.p.A., Milano, Italia. Red fluorescent WGA and Alexa488-phalloidin were from Gibco Invitrogen, USA.

The microfabrication steps to reduce the depth of the microchannels are outlined in Fig. 27. The microchannels were fabricated by micromachining PMMA substrates with the above mentioned micromilling machine. Micromilling is a subtractive microfabricating process that uses rotating cutting tools to remove polymer from a substrate.[53, 95] Such technology has two main functions: realization of masters used in subsequent microfabrication steps; direct fabrication of the microstructures of the final device; in this paper we explored the former. To correlate final and initial depths, we micromilled micron-sized microchannels at different width-depth ratios: 380-200, 380-100, 380-50, 380-25 μm.

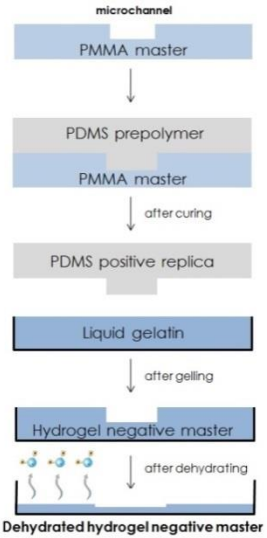


Fig. 28 Schematic illustration of hydrogel dehydration process

Moreover, to show the applicability of the described approach in terms of aspect ratios we micromilled microchannels 100-100 width-depth using a 100 µm microtool and microstructures like pillars, 350-100 µm (width-depth) using a 250 µm microtool. A PMMA bowl 30 x 30 mm and 2 mm depth was fabricated and then used to prepare the hydrogel replica needed to form the final master. To design a draft of the microstructures we created a layout by Draftsight (Cad Software). During micromilling, spindle speed, feed speed and plunge rate per pass were set to 12.000 rpm, 15 mm s-1, and

20, respectively. From PMMA masters with negative features, PDMS positive replica masters were rapidly created using the PDMS thermal curing technique.[51] A typical process involved pouring PDMS mixed in ratio 10:1 with curing agent onto the PMMA microchannel master (Fig. 28 A). Alternatively, it was used a hydrophilic PDMS to facilitate PDMS pre-polymer penetration in the case of more complex structures such as the array of micropillars.[96] In this case the PDMS mixture was then mixed with Silwet L-77 at 4 % wt. In both cases, PDMS precursor was previously exposed to vacuum to eliminate air bubbles for at least 30 min. The PMMA master with PDMS poured was baked in the oven (1 h, 75 °C), to finalize the PDMS curing process (Fig. 28 B). Afterwards, the PMMA bowl was filled with liquid gelatin at defined concentrations, previously degassed with nitrogen for 10 min in order to eliminate bubbles (Fig. 28 C). The hydrophilic or hydrophobic PDMS positive replica was placed onto the gelatin fluid bed in order to obtain a hydrogel negative replica (Fig. 28 D). After a few minutes to stabilize the liquid gelatin the system was put into the fridge for 20 min at 4°C, to finalize the gelling process. After gelling, the PDMS was peeled off from the hydrogel

negative replica ready for the dehydration process (Fig. 28 E). The hydrogel master with the imprint of the PDMS master, was then dried in a controlled environment (temperature 28 °C for 14 h at 200 mbar or 28°C for 36 h) (Fig. 28 G) in which the gel sample dried slowly but uniformly without waves and deformations on the surface (Fig. 28 H). Alternatively, in absence of an oven, the samples can be left at room temperature for 36 h. The entire double replica procedure,[97, 98] using hydrophilic PDMS in the case of micropillars, was repeated to prepare final PDMS microchannels and microstructures arrays with reproducible and down to 3 µm depth limiting the curing temperature of the PDMS at 37 °C to preserve dehydrated hydrogel negative replica in the first replica. To obtain microchannels with aspect ratios (width/depth) down to 3, we explored the reverse process, where the only difference was to imprint gelatin directly with negative PMMA master to prepare a positive gelatin mold. To demonstrate the applicability of the PDMS microchannels replicated onto dehydrated negative gelatin master, these were bonded through oxygen plasma activation to a glass slide

using a plasma chamber (Plasma prep II, SPI) for 1 min at a pressure of 0.3 mbar and power of 37 W. [37]

***Brain endothelial bEnd.3 cells culture*:** In order to allow cell adhesion selectively, array was clamped with a glass coverslip by using a reversible magnetic bonding. The fabricated microstructure reported in Fig. 31 D was sterilized with 10 % penicillin-streptomycin solution in PBS before cell seeding for 24 h at 4 °C to prevent contamination. The rhomboidal areas of the structure within the array were selectively coated with 10 µg/ml fibronectin (Sigma-Aldrich) through capillarity-induced penetration and vacuum for 1 h at 37 °C. Afterwards, the microchannels were washed with PBS to remove fibronectin excess. The glass coverslip was removed under sterile condition and 100 µl of brain endothelial bEnd.3 cell suspension, at a density of 2 × 105 cells/ml in cell culture medium (DMEM + 10% FBS), were seeded on the array. After incubation for cell attachment in a 5 % humidified CO2 incubator at 37 °C, non-adhered cells were removed 2 h after seeding by twice washing with fresh cell culture medium. Afterward, cells were allowed to grow until 3 d within the

device. At this time point, cells were fixed with 4 % paraformaldehyde for 10 min and actin microfilaments and nuclei were stained with Alexa488-phalloidin (Molecular Probes) and DAPI (Sigma), respectively. Samples were observed by multiphoton confocal microscope (Leica TCS SP5 MP) equipped with a 20 × dry objective.

### 4.2.3 Depth shrinking by dehydration process

Motivated by the strong need in µ-TAS and LOC for microchannels thinner than 50 µm, we developed an innovative shrinking approach to obtain microchannels of micrometric depths. Micromilling is one of the oldest microfabrication techniques and to date one of the most used in many laboratories around the world.[99, 100] At the same time several shrinking methods proposed by different research groups have attempted to improve existing microfabrication technologies. In this respect, the main goal of our study was to develop an easy and reproducible method to reduce the manufactured depth associated with micromilling from tens of

micron to few micron. As discussed in this section, we also studied the capability of the proposed method to reduce the fabrication error in the case of depths that can be directly fabricated by micromilling. The investigated method uses mechanical micromachining and soft lithography techniques that are easy, reproducible and inexpensive; it is based on the dehydration of a hydrogel replica inside a laterally confined bowl. This confinement is the reason for the vertical shrinkage of the hydrogel, including the microchannel depth and preservation of the planarity of the final device avoiding any unwished global deformation typical of traditional 3D shrinkage techniques.

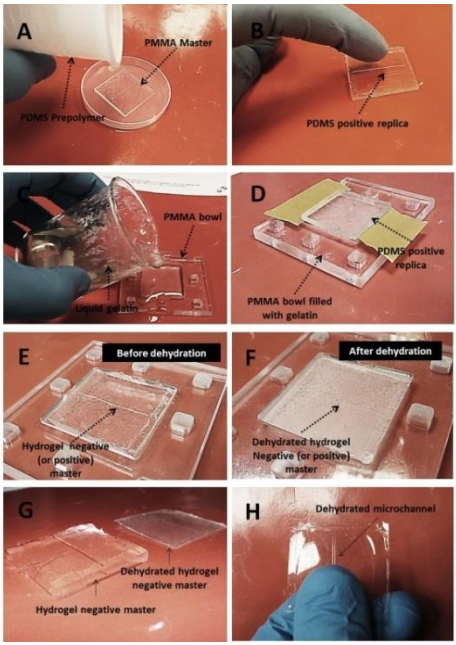


Fig. 29. Preparation of dehydrated hydrogel negative replica.

During the experimental study, we observed that the microchannels obtained using the process, described in Fig. 28, have an enlargement in width of the final microchannel, though with acceptable aspect ratios. Conversely, by dehydrating a positive gelatin replica it was possible to obtain microchannels with a shrunk width and a lower dimensional aspect ratio (width/depth). The first advantage of our hydrogel dehydration process is its simplicity. The

photolithography process comprises spin-coating, pre-baking, UV exposure, post-baking and developing.[101] In contrast, the proposed method only requires a micromilling machine, or other simple mill technologies; the process is finalized within an oven with controlled temperature (28 °C) and vacuum. The oven can also be skipped affecting only the dehydration time, but not the final result (36 h vs. 14 h). As first experimental study a gelatin solution 12 w/v % was used to obtain a hydrogel negative replica with the imprint of the initial PMMA master at different width-depth ratios. The initial depths of the microchannels after micromilling fabrication were, respectively, 240, 160, 55 and 30 µm as reported in Fig. 29. In order to characterize these depths, PDMS replicas realized directly from the initial PMMA masters were measured by using a profilometer. For the profilometer characterization we used a standard scan type on hills profile, a stylus type radius of 2,5 µm and a Meas range of 65,5 or 6,5 µm depending on the final depth. To quantify the depth reduction obtained with the proposed approach we profiled the PDMS replicas fabricated from the dehydrated hydrogel masters. The hydrogel mold obtained after dehydration showed about 88%

of shrinkage in depth from the size of freshly fabricated hydrogel molds, as shown by the profile graphs. Tab. 1 in figure 29 reports the shrinking depth obtained by the differently sized microchannels. At the end of the process, a depth reduction of 88% was confirmed for each microchannel. The results summarized in the table show an almost linear dependence of the shrunk up on the initial depth; a minimum microchannel depth of 3 µm was obtained by a 30 µm depth microchannel. Then, we tested the same microchannels using another gelatin concentrations corresponding to 18 w/v %. In Fig. 29, shrunk depths are plotted as a function of the initial depths; also in these cases almost linear trend was obtained with 85% of shrinkage. In addition, as expected, we observed that using higher gelatin concentrations (from 12 to 18%) the standard deviation value decreased; indeed, less water had to be removed during the process providing a higher level of control on the process.

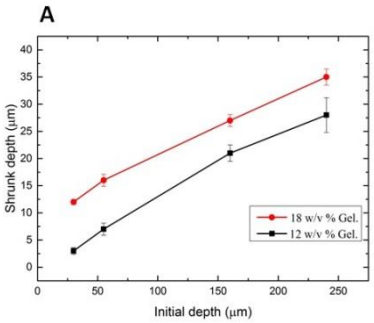


**Table 1.** Srunk depth and related standard deviations

| no | Initial Depth (µm) | Srunk Depth Gel 18 % (µm) | SD Gel 18 % (µm) | Srunk Depth Gel 12 % (µm) | SD Gel 12 % (µm) |
|---|---|---|---|---|---|
| 1 | 240 | 37 | | 31 | |
| 2 | 240 | 35 | 1.52 | 26 | 2.64 |
| 3 | 240 | 34 | | 26 | |
| 4 | 160 | 28 | | 19 | |
| 5 | 160 | 26 | 1.15 | 21 | 1.52 |
| 6 | 160 | 26 | | 22 | |
| 7 | 55 | 15 | | 8,9 | |
| 8 | 55 | 17 | 1.15 | 5,9 | 1.8 |
| 9 | 55 | 17 | | 5,6 | |
| 10 | 30 | 12 | | 3,1 | |
| 11 | 30 | 13 | 0.57 | 2,1 | 0.6 |
| 12 | 30 | 12 | | 3,2 | |

Fig. 30. Effect of initial depth on shrunk depth at different gelatin concentrations.

We also showed capability to fabricate final microchannels with aspect ratios down to 3, dehydrating a positive gelatin mold with a recessed microchannel 100 - 100 µm (width - depth). SEM images of microchannels made of PDMS and obtained respectively by replica from a micromilled PMMA master (100 x 100 µm) and from a dehydrated hydrogel master obtained from the same PMMA master using the two process proposed clearly show the depth reduction and the preservation of the frame thanks to the hydrogel confinement in a PMMA bowl, differently from the shrinkage methods

reported in literature. Final aspect ratios were 20:1 and 3:1, respectively, as indicated in Fig. 30.

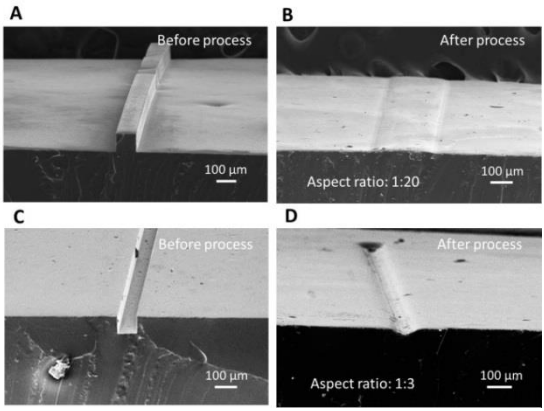


Fig. 31 SEM images of PDMS microchannels before and after process

In addition, our approach is effective in reducing the surface roughness and in manufacturing round profiles. Specifically, roughness profiles by profilometer showed an enhancement of the smoothness since roughness decreases from 156 nm to 24 nm. This significant reduction is highly desirable in microfluidics and it can also be advantageous from an optical standpoint, since the final microchannels result much more transparent and internally inspectable. To show the versatility of the described innovative approach we prepared different discrete microstructures, such as pillars (350 µm in diameter)

and using the proposed process we showed the possibility to reduce the initial depth. Taking advantage from the enlargement of the pillars, we fabricated microchamber arrays connected via microchannels of 5 µm in width starting from arrays of circular pillars. The procedure previously described can be further miniaturized by reducing the diameter of the pillars and the distance between each of them.

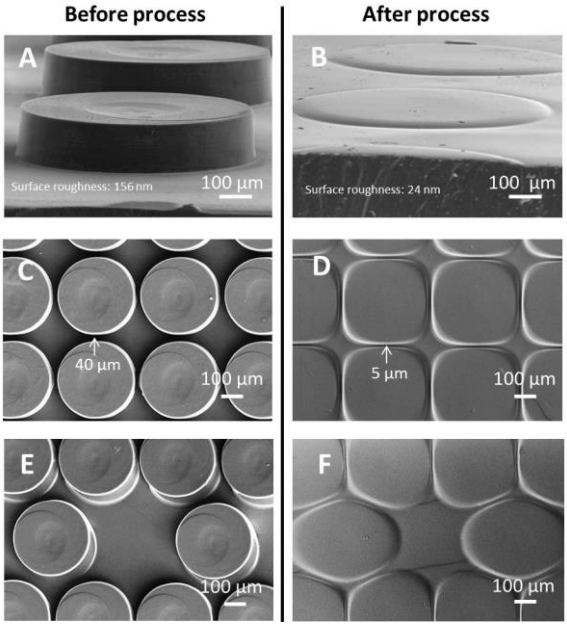


Fig. 32 SEM images, before and after the dehydration process in microstructures like pillars

### 4.2.4 Microchannel validation and microvessel microfabrication

In this section, we provide a comparison, in terms of final error in preparing the same target depth, between direct fabrication by micromilling and the proposed method based on fabrication by micromilling combined with confined gelatin dehydration. Several microfluidic applications require a high level of precision in the microfabrication process for a faithful reproduction of the initial CAD/CAM project. The error of the micromilling process, including the z axis, has been reduced in the last years thanks to higher stage control. However, part of the error in the final depth is due to the manual alignment of the microtool in z of the workpiece, needed to define the coordinate origin.[52, 102] Despite some alignment techniques recently proposed, the fabrication is still affected by an error in z whose impact depends on the final depth: the lower the depth, the higher the relative percentage error. Here, we compared the direct fabrication by micromilling with the proposed method in terms of reproducibility in producing a depth target of 20 μm. The results are summarized in table 2

in figure 32. Variability of the results in the case of direct fabrication by micromilling is evident (SD=11,42), confirming common knowledge. Conversely, depths of PDMS channels obtained with the proposed method resulted in a much higher reproducibility (SD=2.5), since the depths of starting masters being deeper than the final target depths are affected by a more negligible error of the micromilling. For completeness, we also tested the error only due to the shrinkage starting from a PMMA master with fixed depth and as expectable reproducibility was even better (SD=1.6) since in this case the only source of error is in the starting concentration of gelatin in water.

A

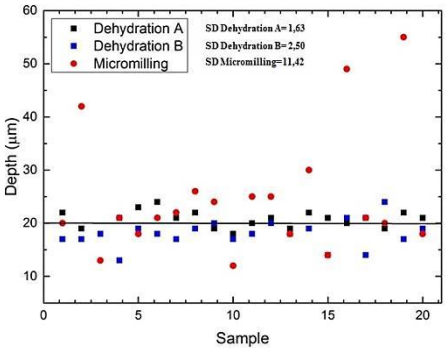


**Table 2.** Direct micromilling fabrication compared to dehydration process in fabricating a microchannel 20 µm depth

| no | Depth Micromilling µm | Depth Dehydration A µm | Depth Dehydration B µm |
|---|---|---|---|
| 1 | 20 | 22 | 17 |
| 2 | 42 | 19 | 17 |
| 3 | 13 | 18 | 18 |
| 4 | 21 | 21 | 13 |
| 5 | 18 | 23 | 19 |
| 6 | 21 | 24 | 18 |
| 7 | 22 | 21 | 17 |
| 8 | 26 | 22 | 19 |
| 9 | 24 | 19 | 20 |
| 10 | 12 | 18 | 17 |
| 11 | 25 | 20 | 18 |
| 12 | 25 | 21 | 20 |
| 13 | 18 | 19 | 18 |
| 14 | 30 | 22 | 19 |
| 15 | 14 | 21 | 14 |
| 16 | 49 | 20 | 21 |
| 17 | 21 | 21 | 14 |
| 18 | 20 | 19 | 24 |
| 19 | 55 | 22 | 17 |
| 20 | 18 | 21 | 19 |

Fig. 33. Fabrication error graph and table of experimental results on micromilling fabrication error.

In addition, microchannels obtained by direct micromilling technology exhibited a high roughness profile, while in many applications a very smooth surface is needed. Interestingly, from the SEM image it is possible to observe the absence of the engraving lines in the case of the mold prepared with the gelatin dehydration approach. This huge reduction in terms of roughness is highly desirable in microfluidics since the final microchannel results much more transparent and internally inspectable. To validate the obtained microchannels we bonded previously described microchannels (aspect ratio 1:20 and 1:3) using the plasma treatment according to the protocol reported in Materials and method (Fig. 33). We fluxed a red aqueous solution containing sulforhodamine B sodium salt at a concentration of 0.1 mg/ml by syringe pump to test the sealing. At the end of the experiment no leakage was observed and a final characterization on the bonded microchannels was performed using a confocal microscope (Leica TCS SP5 MP) with a 25× water-immersion objective. Experimental results confirm that the proposed method can be used for the fabrication of microchannels with a depth down to a few µm (Fig. 33 C-F). As a further applicative

example for the proposed method, rhomboid and hexagonal arrays with reduced depth and connected via 5 µm wide microchannels were fabricated and tested. Recently, some research groups have developed similar geometries to recreate microfluidic logic circuits or for the interrogation and control of cell signalling mechanisms. We were able to obtain the above-mentioned geometries by applying process A onto an array of pillars properly located as shown in Fig. 31. We first tested bonded microstructures inserting by capillarity in a vacuum chamber a red fluorescent liquid. Then, by localizing fibronectin in the shaped areas we assessed capability to confine cells in those areas with no possibility to escape from one to another area due to the small size of the microchannels. To summarize, we demonstrated a novel, simple and reproducible method which does not require advanced and expensive technologies to add value to a low cost technology based on micromilling in terms of miniaturization capability.

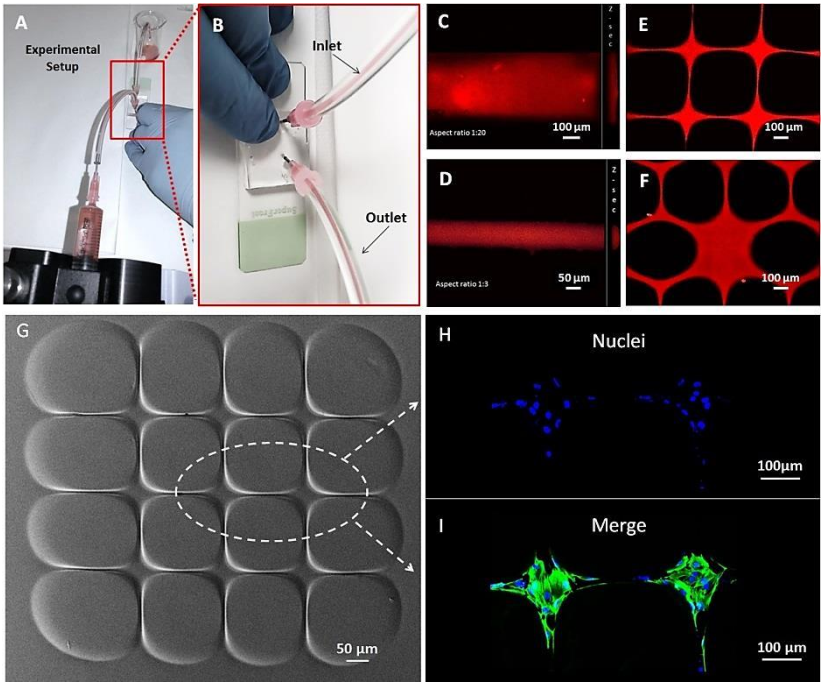


Fig. 34 Validation of the microchannel by flowing a red aqueous solution and culturing bEnd.3 cells

Indeed, the proposed method uses a dehydration process of patterned hydrogel substrates fabricated via replica molding onto micromilled PMMA providing hydrogel masters with demonstrated final micrometric features down to 3 µm for the channel depth and, in specific configurations, down to 5 µm

for the channel width. In addition, the results show that the proposed method is very advantageous in making the preparation of microchannels under 50 µm highly reproducible as compared to direct fabrication by micromilling, as demonstrated choosing 20 µm as target depth. We demonstrated that the extent of reduction can be finely controlled simply by using defined initial depths and hydrogels of varying water content. Some tests on microfluidic devices of reduced size -prepared with the proposed technology- were provided as a validation of the proposed technology. We also used an array of shaped grooves obtained by applying process A on an array of pillars and demonstrated capability to confine cells in those areas thanks to previous localization by capillarity of fibronectin solution through the interconnecting microchannels (Fig. 34). We also showed the possibility to endothelialize the fabricated circular microchannel 8 µm depth (Fig. 35)

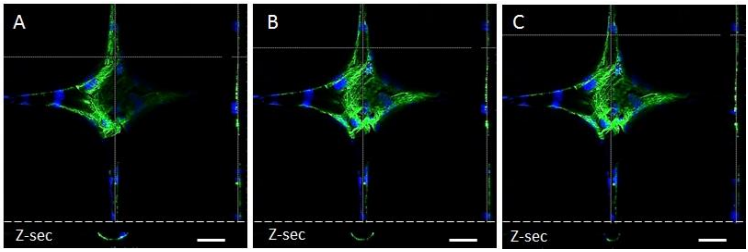


Fig. 35. Endothelialized circular microchannel 8 μm depth.

# 5 “Lab on a chip” practical tips

## 5.1 An easy and fast System for bonding UPCHURCH® NanoPorts to PMMA

Common systems to connect microfluidics devices with classic fluidic equipments (such as syringe or peristaltic pumps) are based on the use of commercial connectors which are not always adaptable for any kind of materials. Upchurch (Oak Harbor, WA, USA) NanoPorts™ Assemblies are the first commercially available products to provide consistent-fluid connectors for chip-based analyses. These patent-pending products bond easily to some-chip surfaces such as glass and polydimethylsiloxane (PDMS) with the provided preformed adhesive rings. All NanoPort™ components are made of inert, biocompatible PEEK™ polymer (nuts and ports) and Perlast® perfluoroelastomer (ferrules and gaskets). However, many microfluidic devices are made of polymethylmetacrilate (PMMA) and in this case the preformed adhesive rings are not suitable. Here, we demonstrate an easy and effective way for the creation of cheap and tight NanoPort Bonding System for

PMMA microdevices. Our approach is a hybrid system which provides the gluing of commercial nanoports with an alternative epoxy adhesive. Also remarkably this is a reusable system, in fact the Flat Bottom Port and the Flat Bottom Port Gasket may be removed and re bonded on another device as explained in the procedure.

***Materials and equipment***

- Fully cured PMMA microchip with via holes to microchannels
- UPCHURCH® SCIENTIFIC NanoPort Assemblies [1]
- Loctite Super Attak Power Flex Gel (5g) or biocompatible glue
- Binder Clip Medium 1-1/4in
- FEP Tubing, 1/16'' x 0.25 mm [2]
- Scalpel and tweezers
- Ethanol
- Hammer

***Fabrication procedure***

We prepared the PMMA surfaces (cleaning with water and drying with an absorbent cloth) and NanoPort™ for bonding. The inlet and outlet holes must be of a diameter below the inner diameter of the Nanoport (around 2 mm) to guaranty no leakage at the interface Nanoport¬PMMA. We put a few drops of Loctite Super Attak Flex Power Gel (5g) on a surface, or a biocompatible glue, in our case we used a piece of PMMA; we took the UPCHURCH® SCIENTIFIC NanoPort, inserted the gasket seal into the recess of the bottom of the port and touched the drop of Loctite Super Attak, in order to deposit the right amount of glue on the bonding surface. Afterwards, we eliminated the excess glue with the aid of a scalpel and attached the flat bottom port gasket directly on the flat bottom port. After this step we took the complete Nanoport (flat bottom port and gasket) and touched the drop of Loctite super attack, eliminating, also in this case,the excess glue with the aid of a scalpel and centering the complete Nanoport on the substrate surrounding the access hole. To finalize the fabrication procedure, we clamped the port to the substrate for 3 h.

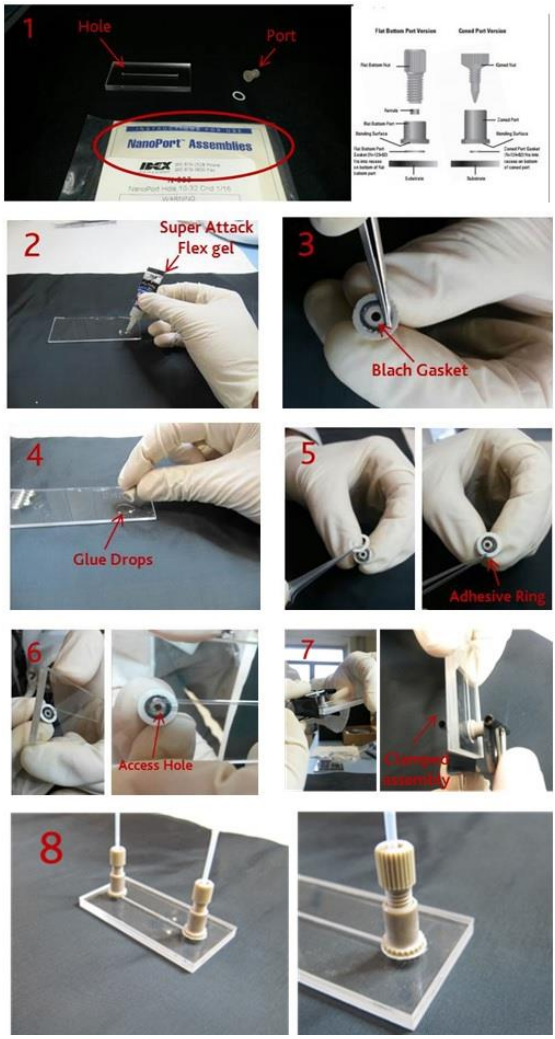


Fig. 36. Bonding UPCHURCH® NanoPorts to PMMA: fabrication procedure

## 5.2 Simple and low cost method to fabricate NOA microfluidic chips

Microfluidic chips are often made of silicon or glass which presents the drawbacks of being relatively expensive, time consuming andlimited in the geometries that can be realized. PMMA is an optimal solution to overcome these aspects but it presents a low chemical resistance to organic solvents and aggressive chemicals. Norland Optical Adhesive 60 ("NOA60") is a clear, colorless, liquid photopolymer that cures when exposed to ultraviolet light. Surface bonding can be activated with light therefore monolithic and transparent devices especially useful for optical elements can be realized. In particular, the use of NOA 60 eliminates premixing, drying, or heat curing operations common to other optical adhesive systems. Curing time is a matter of minutes and is dependent upon the thickness applied and the energy of ultraviolet light available. Dupont and colleagues have recently developed a NOA microfluidic channel via a photolithography multistep method that presents a long time process. Here, we demonstrate the possibility to micromachine already cured

NOA substrates by micromilling that is much easier and cheaper than photolithographic techniques for fabrication of microchannels or microstructures in general. In addition, by micromilling it is possible to easily drill and make open channels in NOA substrates if needed. Also, in the case of microstructures on the two layers to be bonded if one layer presents microstructures with feature sizes below 25 μm and one substrate with feature sizes above this value; then it is possible to prepare one substrate by photolithographic techniques and the other substrate by micromilling with following bonding, saving time and money.

***Materials and equipment***

- Fully cured PDMS mold
- Norland Optical Adhesive 60
- UV light (E-Series Ultraviolet Hand Lamps)
- Micromachining machine
- Oxygen plasma machine
- Clamp

***Fabrication procedure***

We poured liquid photopolymer NOA into a preformed PDMS mold covering the entire surface. After a few minutes to stabilize the liquid polymer we inserted the PDMS mold under UV light for 30 min at a 365 nm wavelength (fig.1B). After the curing time, NOA substrate is ready for the use; we prepared two NOA substrates to fabricate a microfluidic chip. NOA substrates are replicated onto flat PDMS surfaces exploiting the flexibility of the PDMS mold as shown in figures 2A and 2B. Afterwards, we took the NOA substrate and milled a microchannel and related inlet/outlet holes using a micromilling machine (Minitech CNC Mini-Mill) (fig. 3A-3B), to minimize the experimental uncertainty, NOA substrates preformed in point 2 are smoothed before milling. Subsequently, we treated the NOA microchannel and top layer by exposing them to oxygen plasma for 60 s, at a pressure less than 0.1 torr and with a plasma power of 20 W (fig 4A). To finalize the bonding process, we clamped the two substrates, exposing the clamped channel under UV-light for 1 h (fig 4B).

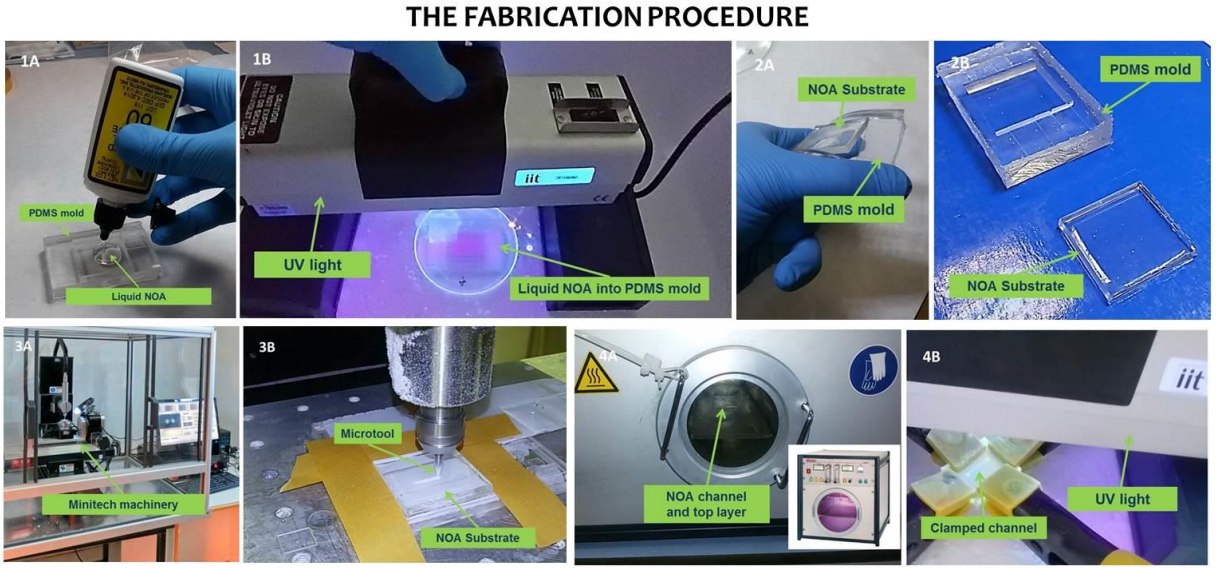


Fig. 37. NOA microfluidic chips: fabrication procedure

## 5.3 Use of gelatin as intermediate thin passivating layer in PDMS soft lithography technology

Microfluidic channels, and microstructures in general, are made by various techniques including photolithography coupled with wet etching, reactive ion etching, stamp-based techniques, such as soft lithography, hot embossing and injection molding, as well as ablation technologies like conventional machining, laser ablation and finally direct 3D printing. Among these techniques, PDMS soft lithography is commonly used to replicate polymer microstructures, and particularly microchannels. Conversely, casting a PDMS replica from a PDMS mold is challenging as both PDMS layers significantly adhere to each other and demoulding is, if at all, only possible after a careful manual cutting and peeling. A less fiddly but more elaborate approach is the passivation of the first PDMS copy by silanisation in order to reduce adhesion. Particularly, in order to prevent adhesion of the PDMS replica on the master, in a conventional process the master is treated with oxygen plasma to activate the surface and immersed for about 2 min into a silane solution (i.e., a mixture of 94% v/v

isopropanol (Sigma Aldrich), 1% v/v acetic acid (Sigma Aldrich), 1% v/v Fluorolink S10 (Solvay), and 4% v/v deionized water) and then placed in an oven at 80 °C for 1 h, thus allowing a complete reaction of the master surface with the fluorinated polymer. This long and expensive process uses materials that are toxic if not removed thoroughly from the master. Recently Gitlin et al. proposed an alternative method utilising hydroxypropylmethylcellulose (HPMC) to passivate a PDMS mold4. Wilson and colleagues presented an “incubation” procedure using a 1% gelatin solution to passivate the PDMS mold, but this method lacks the ability to control the gelatin layer thickness. Our tip shows a precise method for preparing a thin gelatin layer by spin coating technology which helps preserve the geometry of microstructures on the PDMS mold. In addition, the use of the spin coater makes controlling the gelatin thickness easier. Here we propose the use of a thin hydrogel layer created with spin coating technology or other thin layer depositing techniques as a passivating material which is easy to use and less toxic than other passivating materials. In addition, this process yields hydrogel coated

microstructures since gelatin remains on the replicated structures unless it is removed by peel off.

General scheme of the process

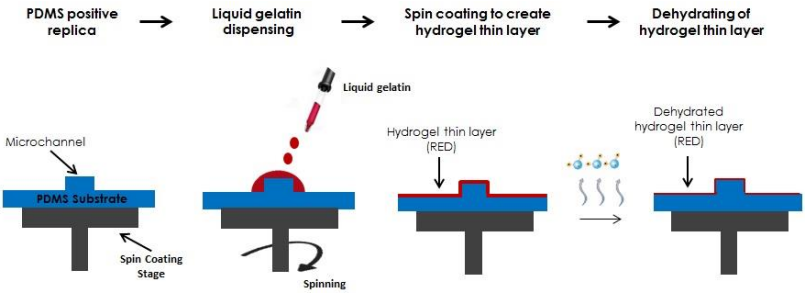


Fig. 38. Scheme of the gelatin process

***Materials and equipment***

- Poly(methyl metacrilate) (PMMA) sheet
- Poly(dimethylsiloxane) PDMS pre-polymer
- Porcine gelatin type A
- Micromachining machine or similar
- Spin coater
- Oxygen plasma machine (optional)
- Tweezers (optional)

***Fabrication procedure***

In the first step we milled microstructures and related inlet/outlet holes (in the case of microchannels) using a micromilling machine (Minitech CNC Mini-Mill) (Fig. 39 1A-B). To design a draft of the microstructures we prepared a layout with Draftsight (Cad Software). During micromilling, spindle speed, feed speed and plunge rate per pass were set to 10 000 rpm, 15 mm/s, and 20, respectively. After micromilling, the PMMA master was ready to use. We poured liquid PDMS prepolymer (10:1) onto the master to fabricate a PDMS positive replica, curing at 80 °C for 2 h (Fig. 39 2A-B). The PDMS precursor was previously exposed to vacuum to eliminate air bubbles for at least 30 min. Afterwards, we placed the PDMS positive replica onto a spin coating stage, depositing a small (~1 ml) droplet of liquid 10% w/v gelatin, previously degassed with nitrogen for 10 min at the center of the substrate and then spinning at high speed (2000 rpm for 20 sec) (Fig. 39 3A-B). Afterwards, we put the system into the fridge for 20 min at 4°C, to finalize the gelling process. At the end of this step we dehydrated the hydrogel layer at room temperature for 5 h under hood aspiration. Alternatively, it is

possible to prepare the gelatin coating via spray deposition. The hydrogel-PDMS positive replica (HPPR) is completely dehydrated and ready to cast a new PDMS replica. Important to notice that we used a curing temperature below 37 °C when making replicas. As optional action, after PDMS curing we removed the dehydrated hydrogel layer with a tweezers from the PDMS negative replica, we also treated the PDMS replica with $O_2$ plasma and bonded the chip to make it ready to use (Fig. 39 4A-B).


Fig. 39. Use of gelatin as intermediate thin passivating layer: fabrication procedure

# 6 Conclusion

In conclusion, in the first part of the thesis, we designed and fabricated a novel PMMA microfluidic system in order to study the effect of flow conditions in controlling the interaction of functionalized nanoparticles with a microfluidic BBB model. We first engineered the microfluidic device inserting a collection chamber to allow the cell growth and the formation of a confluent brain endothelial layer, ensuring the oxygen provision. Furthermore, we integrated an electrode system to control the transepithelial electrical resistance (TEER) during the cell culture. TEER data demonstrate that cells are able to grow and to reach the confluence in the microfluidic system by forming tight junctions, obtaining a plateau value. Moreover, as expected, the presence of the cell layer hinders the transport of albumin and nanoparticles across the porous membrane. More interestingly, the functionalization of nanoparticles with gH625 peptides contributes to enhance the BBB crossing in flow conditions. The flow rate used in our experiments does not affect the cell monolayer integrity as well as the passage of nanoparticles, as reported by TEER

analysis after the experiment. In the second part, applying the same geometry, we reported a simple, fast and low cost procedure to fabricate a reusable microfluidic chip in a hybrid configuration which presents a temporary bonding. The traditional bonding via plasma or solvent evaporation guarantees an irreversible sealing which prevents internal accessibility as well as the reuse of the device. Nowadays, a simple, robust and versatile method to fabricate reusable microfluidic devices is still missing. The proposed hybrid magnet-assisted bonding method is based on the embedding of magnets into the poly(methyl methacrylate) (PMMA) substrates each of them carrying a thin PDMS layer -previously spin coated on the PMMA substrates- which increases the sealing strengthens in flow conditions. Then, an endothelial cell layer was formed by culturing brain endothelial bEnd.3 cells inside the proposed microchannels and characterized in deep upon microchannel aperture which is not otherwise possible with permanently bonded devices. In the "*in vitro* microvessel model" section, we first developed a fast and reproducible method to fabricate polymeric circular microchannels from micromilled square microchannels

coupling a spin coating technology. In particular, a PMDS precursor was deposited by spin coating on the square microchannels and formed a circular shape thanks to surface tension, which smoothed the corners. This PMMA-PDMS master was then used to prepare final semi-circular microchannels by double replica of PDMS, which can be aligned and bonded when closed microchannels are required. This process was useful in making small circular microchannels (down to 50 μm) and it also showed to be effective in creating microchannels with a branched and a ring-shape geometry. Therefore, we proposed a reproducible, versatile, and low cost method to produce open or closed circular microchannels for in vitro vascular microcapillaries that is also useful for other applications such as plug production and microparticle alignment. As a proof of the advantage of producing circular rather than square microchannels, we cultured cells in both devices and verified how the presence of corners negatively affects the growth and uniformity of an endothelial cell layer. Moreover, to scale-down the microchannel dimensions, we demonstrated a novel, simple and reproducible method which does not require advanced and expensive technologies.

Indeed, the proposed method uses a dehydration process of patterned hydrogel substrates fabricated via replica molding onto micromilled PMMA providing hydrogel masters with demonstrated final micrometric features down to 3 µm for the channel depth and, in specific configurations, down to 5 µm for the channel width. In addition, the results show that the proposed method is very advantageous in making the preparation of microchannels under 50 µm highly reproducible as compared to direct fabrication by micromilling, as shown choosing 20 µm as target depth. We demonstrated that the extent of reduction can be finely controlled simply by using defined initial depths and hydrogels of varying water content. Some tests on microfluidic devices of reduced size -prepared with the proposed technology- were provided as a validation of the proposed technology. We also used an array of shaped grooves obtained by applying the proposed process on an array of pillars and demonstrated capability to confine cells in those areas thanks to previous localization by capillarity of fibronectin solution through the interconnecting microchannels. Finally, associated with the development of the above described innovative approaches,

we proposed practical tips to the miniaturization community, developing innovative techniques that offer a solution to commonly encountered problems in the microfabrication field, or improvements (e.g. a simplification) on existing techniques.

# 7 Future outlook

This thesis has explored new approaches to develop microfluidic environments for cell culture. A possible future work, currently under development, includes a new version of these devices, using, for the surrounding microchannels, biomaterials such as gelatin which can better mimic the *in vivo* conditions with the final aim to investigate cell-nanocarriers interactions and answer important biological questions. We particularly imagine that the employment of the gelatin to fabricate a totally gelatin microvessel model, will make a huge impact on "*tissues on chip"* applications. However, one of the main challenges in developing a gelatin microvessel, perfusable and usable in culture conditions, is to avoid the use of protective structures which change the chemical and physical properties of the vessel. Our preliminary experiments show that the process described in 4.1 section can be used to fabricate a gelatin substrate with a semi-circular microchannel which can be scaled down to emulate very small vessels with the approach developed in 4.2 section. For a functioning device, two semi-circular substrates were bonded using the

spin coating process. More experiments need to be performed to find appropriate conditions such as resistance to culture temperature, cross-link degree and cell culture.

# 8 References


1. Whitesides, G. M., The origins and the future of microfluidics. Nature 2006, 442 (7101), 368-373. DOI: 10.1038/nature05058.
2. Haeberle, S.; Zengerle, R., Microfluidic platforms for lab-on-a-chip applications. *Lab on a Chip* **2007,** *7* (9), 1094-1110. DOI: 10.1039/b706364b.
3. Huh, D.; Hamilton, G. A.; Ingber, D. E., From 3D cell culture to organs-on-chips. *Trends in Cell Biology* **2011,** *21* (12), 745-754. DOI: 10.1016/j.tcb.2011.09.005.
4. Jain, K. K., Nanobiotechnology-based strategies for crossing the blood-brain barrier. *Nanomedicine* **2012,** *7* (8), 1225-1233.
5. Booth, R.; Kim, H., Characterization of a microfluidic in vitro model of the blood-brain barrier (mu BBB). *Lab on a Chip* **2012,** *12* (10), 1784-1792. DOI: 10.1039/c2lc40094d.
6. Wilmer, M. J.; Ng, C. P.; Lanz, H. L.; Vulto, P.; Suter-Dick, L.; Masereeuw, R., Kidney-on-a-Chip Technology for Drug-Incuced Nephrotoxiciy Screening. *Trends in Biotechnology* **2016,** *34* (2), 156-170. DOI: 10.1016/j.tibtech.2015.11.001.
7. Crunkhorn, S., Respiratory diseases: Lung airway-on-a-chip. *Nature reviews. Drug discovery* **2016,** *15* (2), 86. DOI: 10.1038/nrd.2016.7.
8. Madou, M. J., Fundamentals of Microfabrication and Nanotechnology. August 1, 2011.
9. Lee, K.; Kim, C.; Shin, K. S.; Lee, J.; Ju, B.-K.; Kim, T. S.; Lee, S.-K.; Kang, J. Y., Fabrication of round channels using the surface tension of PDMS and its application to a 3D serpentine mixer. *Journal of Micromechanics and Microengineering* **2007,** *17* (8), 1533-1541. DOI: 10.1088/0960-1317/17/8/016.
10. Choi, J. S.; Piao, Y.; Seo, T. S., Fabrication of a circular PDMS microchannel for constructing a three-dimensional endothelial

cell layer. *Bioprocess and Biosystems Engineering* **2013,** *36* (12), 1871-1878. DOI: 10.1007/s00449-013-0961-z.
11. Chisti, Y., Hydrodynamic damage to animal cells. *Critical Reviews in Biotechnology* **2001,** *21* (2), 67-110. DOI: 10.1080/20013891081692.
12. Leclerc, E.; Sakai, Y.; Fujii, T., Cell culture in 3-dimensional microfluidic structure of PDMS (polydimethylsiloxane). *Biomedical Microdevices* **2003,** *5* (2), 109-114. DOI: 10.1023/a:1024583026925.
13. Walker, G. M.; Zeringue, H. C.; Beebe, D. J., Microenvironment design considerations for cellular scale studies. *Lab on a Chip* **2004,** *4* (2), 91-97. DOI: 10.1039/b311214d.
14. Keane, J. T.; Ryan, D.; Gray, P. P., Effect of shear stress on expression of a recombinant protein by Chinese hamster ovary cells. *Biotechnology and Bioengineering* **2003,** *81* (2), 211-220. DOI: 10.1002/bit.10472.
15. Kamm, R. D., Cellular fluid mechanics. *Annual Review of Fluid Mechanics* **2002,** *34*, 211-232. DOI: 10.1146/annurev.fluid.34.082401.165302.
16. Sugihara-Seki, M., Flow around cells adhered to a microvessel wall. I. Fluid stresses and forces acting on the cells. *Biorheology* **2000,** *37* (5-6), 341-359.
17. Sugihara-Seki, M., Flow around cells adhered to a microvessel wall II: Comparison to flow around adherent cells in channel flow. *Biorheology* **2001,** *38* (1), 3-13.
18. Rathore, A. S.; Reynolds, K. J.; Colon, L. A., Joule heating in packed capillaries used in capillary electrochromotography. *Electrophoresis* **2002,** *23* (17), 2918-2928. DOI: 10.1002/1522-2683(200209)23:17<2918::aid-elps2918>3.0.co;2-c.
19. Lin, Y. C.; Huang, M. Y.; Young, K. C.; Chang, T. T.; Wu, C. Y., A rapid micro-polymerase chain reaction system for hepatitis C virus amplification. *Sensors and Actuators B-Chemical* **2000,** *71* (1-2), 2-8. DOI: 10.1016/s0925-4005(00)00558-x.

20. Beebe, D. J.; Mensing, G. A.; Walker, G. M., Physics and applications of microfluidics in biology. *Annual Review of Biomedical Engineering* **2002,** *4*, 261-286. DOI: 10.1146/annurev.bioeng.4.112601.125916.
21. Walker, G. M.; Ozers, M. S.; Beebe, D. J., Insect cell culture in microfluidic channels. *Biomedical Microdevices* **2002,** *4* (3), 161-166. DOI: 10.1023/a:1016088128057.
22. Soper, S. A.; Henry, A. C.; Vaidya, B.; Galloway, M.; Wabuyele, M.; McCarley, R. L., Surface modification of polymer-based microfluidic devices. *Analytica Chimica Acta* **2002,** *470* (1), 87-99. DOI: 10.1016/s0003-2670(02)00356-2.
23. Hu, S. W.; Ren, X. Q.; Bachman, M.; Sims, C. E.; Li, G. P.; Allbritton, N., Surface modification of poly(dimethylsiloxane) microfluidic devices by ultraviolet polymer grafting. *Analytical Chemistry* **2002,** *74* (16), 4117-4123. DOI: 10.1021/ac025700w.
24. Balaban, N. Q.; Schwarz, U. S.; Riveline, D.; Goichberg, P.; Tzur, G.; Sabanay, I.; Mahalu, D.; Safran, S.; Bershadsky, A.; Addadi, L.; Geiger, B., Force and focal adhesion assembly: a close relationship studied using elastic micropatterned substrates. *Nature Cell Biology* **2001,** *3* (5), 466-472. DOI: 10.1038/35074532.
25. Teixeira, A. I.; Abrams, G. A.; Bertics, P. J.; Murphy, C. J.; Nealey, P. F., Epithelial contact guidance on well-defined micro- and nanostructured substrates. *Journal of Cell Science* **2003,** *116* (10), 1881-1892. DOI: 10.1242/jcs.00383.
26. Walboomers, X. F.; Croes, H. J. E.; Ginsel, L. A.; Jansen, J. A., Growth behavior of fibroblasts on microgrooved polystyrene. *Biomaterials* **1998,** *19* (20), 1861-1868. DOI: 10.1016/s0142-9612(98)00093-3.
27. Chang, S.; Popowich, Y.; Greco, R. S.; Haimovich, B., Neutrophil survival on biomaterials is determined by surface topography. *Journal of Vascular Surgery* **2003,** *37* (5), 1082-1090. DOI: 10.1067/mva.2003.160.

28. Elliott, J. T.; Tona, A.; Woodward, J. T.; Jones, P. L.; Plant, A. L., Thin films of collagen affect smooth muscle cell morphology. *Langmuir* **2003,** *19* (5), 1506-1514. DOI: 10.1021/la026216r.
29. Brakebusch, C.; Fassler, R., The integrin-actin connection, an eternal love affair. *Embo Journal* **2003,** *22* (10), 2324-2333. DOI: 10.1093/emboj/cdg245.
30. Pribila, J. T.; Shimizu, Y., Signal transduction events regulating integrin function and T cell migration - New functions and complexity. *Immunologic Research* **2003,** *27* (1), 107-128. DOI: 10.1385/ir:27:1:107.
31. Chen, C. S.; Alonso, J. L.; Ostuni, E.; Whitesides, G. M.; Ingber, D. E., Cell shape provides global control of focal adhesion assembly. *Biochemical and Biophysical Research Communications* **2003,** *307* (2), 355-361. DOI: 10.1016/s0006-291x(03)01165-3.
32. Nelson, C. M.; Chen, C. S., Cell-cell signaling by direct contact increases cell proliferation via a PI3K-dependent signal. *Febs Letters* **2002,** *514* (2-3), 238-242. DOI: 10.1016/s0014-5793(02)02370-0.
33. Zhu, Z.; Matthews, I. P.; Wang, C., Gas dynamics of ethylene oxide during sterilization. *Review of Scientific Instruments* **1999,** *70* (7), 3150-3155. DOI: 10.1063/1.1149878.
34. Shintani, H., Effects of ionizing radiation sterilization treatment on medical use plastic materials. *Biocontrol Science* **2002,** *7* (1), 1-8.
35. Whitesides, G. M.; Ostuni, E.; Takayama, S.; Jiang, X. Y.; Ingber, D. E., Soft lithography in biology and biochemistry. *Annual Review of Biomedical Engineering* **2001,** *3*, 335-373. DOI: 10.1146/annurev.bioeng.3.1.335.
36. Mata, A.; Fleischman, A. J.; Roy, S., Characterization of polydimethylsiloxane (PDMS) properties for biomedical micro/nanosystems. *Biomedical Microdevices* **2005,** *7* (4), 281-293. DOI: 10.1007/s10544-005-6070-2.
37. Bhattacharya, S.; Datta, A.; Berg, J. M.; Gangopadhyay, S., Studies on surface wettability of poly(dimethyl) siloxane (PDMS)

and glass under oxygen-plasma treatment and correlation with bond strength. *Journal of Microelectromechanical Systems* **2005,** *14* (3), 590-597. DOI: 10.1109/jmems.2005.844746.
38. Kim, P.; Kwon, K. W.; Park, M. C.; Lee, S. H.; Kim, S. M.; Suh, K. Y., Soft lithography for microfluidics: a review. *Biochip Journal* **2008,** *2* (1), 1-11.
39. Chen, C. S.; Breslauer, D. N.; Luna, J. I.; Grimes, A.; Chin, W. C.; Leeb, L. P.; Khine, M., Shrinky-Dink microfluidics: 3D polystyrene chips. *Lab on a Chip* **2008,** *8* (4), 622-624. DOI: 10.1039/b719029h.
40. Shim, J.; Bersano-Begey, T. F.; Zhu, X. Y.; Tkaczyk, A. H.; Linderman, J. J.; Takayama, S., Micro- and nanotechnologies for studying cellular function. *Current Topics in Medicinal Chemistry* **2003,** *3* (6), 687-703. DOI: 10.2174/1568026033452393.
41. Takayama, S.; Ostuni, E.; LeDuc, P.; Naruse, K.; Ingber, D. E.; Whitesides, G. M., Selective chemical treatment of cellular microdomains using multiple laminar streams. *Chemistry & Biology* **2003,** *10* (2), 123-130. DOI: 10.1016/s1074-5521(03)00019-x.
42. Huang, Z.; Li, X.; Martins-Green, M.; Liu, Y., Microfabrication of cylindrical microfluidic channel networks for microvascular research. *Biomedical Microdevices* **2012,** *14* (5), 873-883. DOI: 10.1007/s10544-012-9667-2.
43. Borenstein, J. T.; Tupper, M. M.; Mack, P. J.; Weinberg, E. J.; Khalil, A. S.; Hsiao, J.; Garcia-Cardena, G., Functional endothelialized microvascular networks with circular cross-sections in a tissue culture substrate. *Biomedical Microdevices* **2010,** *12* (1), 71-79. DOI: 10.1007/s10544-009-9361-1.
44. Becker, H.; Gartner, C., Polymer microfabrication methods for microfluidic analytical applications. *Electrophoresis* **2000,** *21* (1), 12-26. DOI: 10.1002/(sici)1522-2683(20000101)21:1<12::aid-elps12>3.3.co;2-z.

45. Becker, H.; Gartner, C., Polymer microfabrication technologies for microfluidic systems. *Analytical and Bioanalytical Chemistry* **2008,** *390* (1), 89-111. DOI: 10.1007/s00216-007-1692-2.
46. Alrifaiy, A.; Lindahl, O. A.; Ramser, K., Polymer-Based Microfluidic Devices for Pharmacy, Biology and Tissue Engineering. *Polymers* **2012,** *4* (3), 1349-1398. DOI: 10.3390/polym4031349.
47. Ehrfeld, W.; Hessel, V.; Lowe, H.; Schulz, C.; Weber, L., Materials of LIGA technology. *Microsystem Technologies* **1999,** *5* (3), 105-112. DOI: 10.1007/s005420050150.
48. Martynova, L.; Locascio, L. E.; Gaitan, M.; Kramer, G. W.; Christensen, R. G.; MacCrehan, W. A., Fabrication of plastic microfluid channels by imprinting methods. *Analytical Chemistry* **1997,** *69* (23), 4783-4789. DOI: 10.1021/ac970558y.
49. Piotter, V.; Hanemann, T.; Ruprecht, R.; Hausselt, J., Injection molding and related techniques for fabrication of microstructures. *Microsystem Technologies* **1997,** *3* (3), 129-133. DOI: 10.1007/s005420050069.
50. Xia, Y. N.; Whitesides, G. M., Soft lithography. *Angewandte Chemie-International Edition* **1998,** *37* (5), 550-575. DOI: 10.1002/(sici)1521-3773(19980316)37:5<550::aid-anie550>3.0.co;2-g.
51. Brittain, S.; Paul, K.; Zhao, X. M.; Whitesides, G., Soft lithography and microfabrication. *Physics World* **1998,** *11* (5), 31-36.
52. Chae, J.; Park, S. S.; Freiheit, T., Investigation of micro-cutting operations. *International Journal of Machine Tools & Manufacture* **2006,** *46* (3-4), 313-332. DOI: 10.1016/j.ijmachtools.2005.05.015.
53. Guckenberger, D. J.; de Groot, T. E.; Wan, A. M. D.; Beebe, D. J.; Young, E. W. K., Micromilling: a method for ultra-rapid prototyping of plastic microfluidic devices. *Lab on a Chip* **2015,** *15* (11), 2364-2378. DOI: 10.1039/c5lc00234f.
54. Tsao, C.-W.; DeVoe, D. L., Bonding of thermoplastic polymer microfluidics. *Microfluidics and Nanofluidics* **2009,** *6* (1), 1-16. DOI: 10.1007/s10404-008-0361-x.

55. Rotting, O.; Ropke, W.; Becker, H.; Gartner, C., Polymer microfabrication technologies. *Microsystem Technologies* **2002,** *8* (1), 32-36. DOI: 10.1007/s00542-002-0106-9.
56. Chen, Z. F.; Gao, Y. H.; Su, R. G.; Li, C. W.; Lin, J. M., Fabrication and characterization of poly(methyl methacrylate) microchannels by in situ polymerization with a novel metal template. *Electrophoresis* **2003,** *24* (18), 3246-3252. DOI: 10.1002/elps.200305534.
57. Kelly, R. T.; Pan, T.; Woolley, A. T., Phase-changing sacrificial materials for solvent bonding of high-performance polymeric capillary electrophoresis microchips. *Analytical Chemistry* **2005,** *77* (11), 3536-3541. DOI: 10.1021/ac0501083.
58. Klank, H.; Kutter, J. P.; Geschke, O., CO2-laser micromachining and back-end processing for rapid production of PMMA-based microfluidic systems. *Lab on a Chip* **2002,** *2* (4), 242-246. DOI: 10.1039/b206409j.
59. Pardridge, W. M., The blood-brain barrier: bottleneck in brain drug development. *NeuroRx : the journal of the American Society for Experimental NeuroTherapeutics* **2005,** *2* (1), 3-14. DOI: 10.1602/neurorx.2.1.3.
60. Ballabh, P.; Braun, A.; Nedergaard, M., The blood-brain barrier: an overview - Structure, regulation, and clinical implications. *Neurobiology of Disease* **2004,** *16* (1), 1-13. DOI: 10.1016/j.nbd.2003.12.016.
61. Deli, M. A.; Abraham, C. S.; Kataoka, Y.; Niwa, M., Permeability studies on in vitro blood-brain barrier models: Physiology, pathology, and pharmacology. *Cellular and Molecular Neurobiology* **2005,** *25* (1), 59-127. DOI: 10.1007/s10571-004-1377-8.
62. Brightman, M. W.; Reese, T. S., Junctions between intimately apposed cell membranes in the vertebrate brain. *The Journal of cell biology* **1969,** *40* (3), 648-77. DOI: 10.1083/jcb.40.3.648.
63. Pardridge, W. M., Blood-brain barrier delivery. *Drug Discovery Today* **2007,** *12* (1-2), 54-61. DOI: 10.1016/j.drudis.2006.10.013.

64. Cucullo, L.; Aumayr, B.; Rapp, E.; Janigro, D., Drug delivery and in vitro models of the blood-brain barrier. *Current Opinion in Drug Discovery & Development* **2005,** *8* (1), 89-99.
65. Guarnieri, D.; Falanga, A.; Muscetti, O.; Tarallo, R.; Fusco, S.; Galdiero, M.; Galdiero, S.; Netti, P. A., Shuttle-Mediated Nanoparticle Delivery to the Blood-Brain Barrier. *Small* **2013,** *9* (6), 853-862. DOI: 10.1002/smll.201201870.
66. Griep, L. M.; Wolbers, F.; de Wagenaar, B.; ter Braak, P. M.; Weksler, B. B.; Romero, I. A.; Couraud, P. O.; Vermes, I.; van der Meer, A. D.; van den Berg, A., BBB ON CHIP: microfluidic platform to mechanically and biochemically modulate blood-brain barrier function. *Biomedical Microdevices* **2013,** *15* (1), 145-150. DOI: 10.1007/s10544-012-9699-7.
67. Petronis, S.; Stangegaard, M.; Christensen, C. B. V.; Dufva, M., Transparent polymeric cell culture chip with integrated temperature control and uniform media perfusion. *Biotechniques* **2006,** *40* (3), 368-376. DOI: 10.2144/000112122.
68. Ziolkowska, K.; Kwapiszewski, R.; Brzozka, Z., Microfluidic devices as tools for mimicking the in vivo environment. *New Journal of Chemistry* **2011,** *35* (5), 979-990. DOI: 10.1039/c0nj00709a.
69. Barreto, J. A.; O'Malley, W.; Kubeil, M.; Graham, B.; Stephan, H.; Spiccia, L., Nanomaterials: Applications in Cancer Imaging and Therapy. *Advanced Materials* **2011,** *23* (12), H18-H40. DOI: 10.1002/adma.201100140.
70. Rasponi, M.; Piraino, F.; Sadr, N.; Lagana, M.; Redaelli, A.; Moretti, M., Reliable magnetic reversible assembly of complex microfluidic devices: fabrication, characterization, and biological validation. *Microfluidics and Nanofluidics* **2011,** *10* (5), 1097-1107. DOI: 10.1007/s10404-010-0738-5.
71. Lu, J. C.; Liao, W. H.; Tung, Y. C., Magnet-assisted device-level alignment for the fabrication of membrane-sandwiched polydimethylsiloxane microfluidic devices. *Journal of Micromechanics and Microengineering* **2012,** *22* (7). DOI: 10.1088/0960-1317/22/7/075006.

72. Valencia, P. M.; Farokhzad, O. C.; Karnik, R.; Langer, R., Microfluidic technologies for accelerating the clinical translation of nanoparticles. *Nature Nanotechnology* **2012,** *7* (10), 623-629. DOI: 10.1038/nnano.2012.168.
73. Andersson, H.; van den Berg, A., Microfluidic devices for cellomics: a review. *Sensors and Actuators B-Chemical* **2003,** *92* (3), 315-325. DOI: 10.1016/s0925-4005(03)00266-1.
74. Lee, J. S., 1998 distinguished lecture: Biomechanics of the microcirculation, an integrative and therapeutic perspective. *Annals of Biomedical Engineering* **2000,** *28* (1), 1-13. DOI: 10.1114/1.249.
75. Miller, J. S.; Stevens, K. R.; Yang, M. T.; Baker, B. M.; Nguyen, D.-H. T.; Cohen, D. M.; Toro, E.; Chen, A. A.; Galie, P. A.; Yu, X.; Chaturvedi, R.; Bhatia, S. N.; Chen, C. S., Rapid casting of patterned vascular networks for perfusable engineered three-dimensional tissues. *Nature Materials* **2012,** *11* (9), 768-774. DOI: 10.1038/nmat3357.
76. Seo, J.; Ionescu-Zanetti, C.; Diamond, J.; Lal, R.; Lee, L. P., Integrated multiple patch-clamp array chip via lateral cell trapping junctions. *Applied Physics Letters* **2004,** *84* (11), 1973-1975. DOI: 10.1063/1.1650035.
77. Dendukuri, D.; Gu, S. S.; Pregibon, D. C.; Hatton, T. A.; Doyle, P. S., Stop-flow lithography in a microfluidic device. *Lab on a Chip* **2007,** *7* (7), 818-828. DOI: 10.1039/b703457a.
78. D'Avino, G.; Romeo, G.; Villone, M. M.; Greco, F.; Netti, P. A.; Maffettone, P. L., Single line particle focusing induced by viscoelasticity of the suspending liquid: theory, experiments and simulations to design a micropipe flow-focuser. *Lab on a Chip* **2012,** *12* (9), 1638-1645. DOI: 10.1039/c2lc21154h.
79. Fiorini, G. S.; Chiu, D. T., Disposable microfluidic devices: fabrication, function, and application. *Biotechniques* **2005,** *38* (3), 429-446. DOI: 10.2144/05383rv02.
80. Abdelgawad, M.; Wu, C.; Chien, W. Y.; Geddie, W. R.; Jewett, M. A. S.; Sun, Y., A fast and simple method to fabricate circular

microchannels in polydimethylsiloxane (PDMS). *Lab on a Chip* **2011,** *11* (3), 545-551. DOI: 10.1039/c0lc00093k.
81. Shih, T.-K.; Chen, C.-F.; Ho, J.-R.; Chuang, F.-T., Fabrication of PDMS (polydimethylsiloxane) microlens and diffuser using replica molding. *Microelectronic Engineering* **2006,** *83* (11-12), 2499-2503. DOI: 10.1016/j.mee.2006.05.006.
82. De Ville, M.; Coquet, P.; Brunet, P.; Boukherroub, R., Simple and low-cost fabrication of PDMS microfluidic round channels by surface-wetting parameters optimization. *Microfluidics and Nanofluidics* **2012,** *12* (6), 953-961. DOI: 10.1007/s10404-011-0929-8.
83. Salic, A.; Tusek, A.; Zelic, B., Application of microreactors in medicine and biomedicine. *Journal of Applied Biomedicine* **2012,** *10* (3), 137-153. DOI: 10.2478/v10136-012-0011-1.
84. Delamarche, E.; Juncker, D.; Schmid, H., Microfluidics for processing surfaces and miniaturizing biological assays. *Advanced Materials* **2005,** *17* (24), 2911-2933. DOI: 10.1002/adma.200501129.
85. Hwang, D. K.; Dendukuri, D.; Doyle, P. S., Microfluidic-based synthesis of non-spherical magnetic hydrogel microparticles. *Lab on a Chip* **2008,** *8* (10), 1640-1647. DOI: 10.1039/b805176c.
86. Bousse, L.; Mouradian, S.; Minalla, A.; Yee, H.; Williams, K.; Dubrow, R., Protein sizing on a microchip. *Analytical Chemistry* **2001,** *73* (6), 1207-1212. DOI: 10.1021/ac0012492.
87. Bogorad, M. I., Review: in vitro microvessel models. Jackson DeStefano, J. K., Andrew D. Wong, Sharon Gerecht and Peter C. Searson, Ed. Lab on a Chip: Lab on a Chip, 2015; pp 4242-4255. DOI: 10.1039/C5LC00832H.
88. Sundberg, S. A., High-throughput and ultra-high-throughput screening: solution- and cell-based approaches. *Current Opinion in Biotechnology* **2000,** *11* (1), 47-53. DOI: 10.1016/s0958-1669(99)00051-8.

89. Bennett, M. R.; Hasty, J., Microfluidic devices for measuring gene network dynamics in single cells. *Nature Reviews Genetics* **2009,** *10* (9), 628-638. DOI: 10.1038/nrg2625.
90. Zare, R. N.; Kim, S., Microfluidic Platforms for Single-Cell Analysis. In *Annual Review of Biomedical Engineering, Vol 12*, Yarmush, M. L.; Duncan, J. S.; Gray, M. L., Eds. Annual Reviews: Palo Alto, 2010; Vol. 12, pp 187-201. DOI: 10.1146/annurev-bioeng-070909-105238.
91. Cao, H.; Tegenfeldt, J. O.; Austin, R. H.; Chou, S. Y., Gradient nanostructures for interfacing microfluidics and nanofluidics. *Applied Physics Letters* **2002,** *81* (16), 3058-3060. DOI: 10.1063/1.1515115.
92. Focaroli, S.; Mazzitelli, S.; Falconi, M.; Luca, G.; Nastruzzi, C., Preparation and validation of low cost microfluidic chips using a shrinking approach. *Lab on a Chip* **2014,** *14* (20), 4007-4016. DOI: 10.1039/c4lc00679h.
93. Das, A. L.; Mukherjee, R.; Katiyer, V.; Kulkarni, M.; Ghatak, A.; Sharma, A., Generation of sub-micrometer-scale patterns by successive miniaturization using hydrogels. *Advanced Materials* **2007,** *19* (15), 1943-+. DOI: 10.1002/adma.200602681.
94. de Oliveira, F. B.; Rodrigues, A. R.; Coelho, R. T.; de Souza, A. F., Size effect and minimum chip thickness in micromilling. *International Journal of Machine Tools & Manufacture* **2015,** *89*, 39-54. DOI: 10.1016/j.ijmachtools.2014.11.001.
95. Chen, P. C.; Pan, C. W.; Lee, W. C.; Li, K. M., An experimental study of micromilling parameters to manufacture microchannels on a PMMA substrate. *International Journal of Advanced Manufacturing Technology* **2014,** *71* (9-12), 1623-1630. DOI: 10.1007/s00170-013-5555-z.
96. Yang, W.; Nam, Y. G.; Lee, B.-K.; Han, K.; Kwon, T. H.; Kim, D. S., Fabrication of a Hydrophilic Poly(dimethylsiloxane) Microporous Structure and Its Application to Portable Microfluidic Pump. *Japanese Journal of Applied Physics* **2010,** *49* (6). DOI: 10.1143/jjap.49.06gm01.

97. Occhipinti, L. G., Surface treatment of an organic or inorganic substrate for enhancing stability of a lithographically defined deposited metal layer Porro, F., Ed. US Pat. App. 12/835,011 2010; Vol. US Pat. App. 12/835,011
98. Zhao, X. M.; Xia, Y. N.; Whitesides, G. M., Soft lithographic methods for nano-fabrication. *Journal of Materials Chemistry* **1997,** *7* (7), 1069-1074. DOI: 10.1039/a700145b.
99. Spath, D.; Tritschler, H.; Bischoff, L.; Schulz, W., Micromilling - High potential technology for micromechanical parts. *Amst 02: Advanced Manufacturing Systems and Technology, Proceedings* **2002,** (437), 859-864.
100. Okano, K., MICROMACHINING OF MICROMACHINE PARTS. *International Journal of the Japan Society for Precision Engineering* **1994,** *28* (3), 196-199.
101. Pimpin, A., Review on Micro- and Nanolithography Techniques and their Applications. *ENGINEERING JOURNAL* **2011,** *16* (1). DOI: 10.4186/ej.2012.16.1.37.
102. Lee, K.; Dornfeld, D. A.; Sme, An experimental study on burr formation in micro milling aluminum and copper. *Transactions of the North American Manufacturing Research Institute of Sme, Vol Xxx, 2002* **2002**, 255-262.